

RESEARCH

Open Access



Mapping snoRNA-target RNA interactions in an RNA-binding protein-dependent manner with chimeric eCLIP

Zhuoyi Song^{1†}, Bongmin Bae^{2†}, Simon Schnabl², Fei Yuan¹, Thareendra De Zoysa², Maureen V. Akinyi¹, Charlotte A. Le Roux¹, Karine Choquet³, Amanda J. Whipple^{2*} and Eric L. Van Nostrand^{1*}

[†]Zhuoyi Song and Bongmin Bae contributed equally to this work.

*Correspondence: amanda_whipple@fas.harvard.edu; eric.vannostrand@bcm.edu

¹Therapeutic Innovation Center & the Verna Marris McLean Department of Biochemistry & Molecular Pharmacology, Baylor College of Medicine, Houston, TX, USA

²Department of Molecular & Cellular Biology, Harvard University, Cambridge, MA, USA

³Department of Biochemistry and Functional Genomics, Université de Sherbrooke, Sherbrooke, Québec, Canada

Abstract

Background: Small nucleolar RNAs (snoRNAs) are non-coding RNAs that function in ribosome and spliceosome biogenesis, primarily by guiding modifying enzymes to specific sites on ribosomal RNA (rRNA) and spliceosomal RNA (snRNA). However, many orphan snoRNAs remain uncharacterized, with unidentified or unvalidated targets, and studies on additional snoRNA-associated proteins are limited.

Results: We adapted an enhanced chimeric eCLIP approach to comprehensively profile snoRNA-target RNA interactions using both core and accessory snoRNA-binding proteins as baits. Using core snoRNA-binding proteins, we confirmed most annotated snoRNA-rRNA and snoRNA-snRNA interactions in mouse and human cell lines and called novel, high-confidence interactions for orphan snoRNAs. While some of these interactions result in chemical modification, others may have modification-independent functions. We showed that snoRNA ribonucleoprotein complexes containing certain accessory proteins, like WDR43 and NOLC1, enriched for specific subsets of snoRNA-target RNA interactions with distinct roles in ribosome and spliceosome biogenesis. Notably, we discovered that SNORD89 guides 2'-O-methylation at two neighboring sites in U2 snRNA that fine-tune splice site recognition.

Conclusions: Chimeric eCLIP of snoRNA-associating proteins enables a comprehensive framework for studying snoRNA-target interactions in an RNA-binding protein-dependent manner, revealing novel interactions and regulatory roles in RNA biogenesis.

Background

Small nucleolar RNAs (snoRNAs) constitute a class of non-coding RNAs primarily known for their fundamental roles in ensuring the proper biogenesis of ribosomal RNA (rRNA). SnoRNAs can be categorized into box C/D and box H/ACA snoRNAs, distinguished by the presence of conserved box motif sequences and structural features. In addition, a class of snoRNAs known as small Cajal body-specific snoRNAs (scaRNAs), which contain either



© The Author(s) 2025. **Open Access** This article is licensed under a Creative Commons Attribution-NonCommercial-NoDerivatives 4.0 International License, which permits any non-commercial use, sharing, distribution and reproduction in any medium or format, as long as you give appropriate credit to the original author(s) and the source, provide a link to the Creative Commons licence, and indicate if you modified the licensed material. You do not have permission under this licence to share adapted material derived from this article or parts of it. The images or other third party material in this article are included in the article's Creative Commons licence, unless indicated otherwise in a credit line to the material. If material is not included in the article's Creative Commons licence and your intended use is not permitted by statutory regulation or exceeds the permitted use, you will need to obtain permission directly from the copyright holder. To view a copy of this licence, visit <http://creativecommons.org/licenses/by-nc-nd/4.0/>.

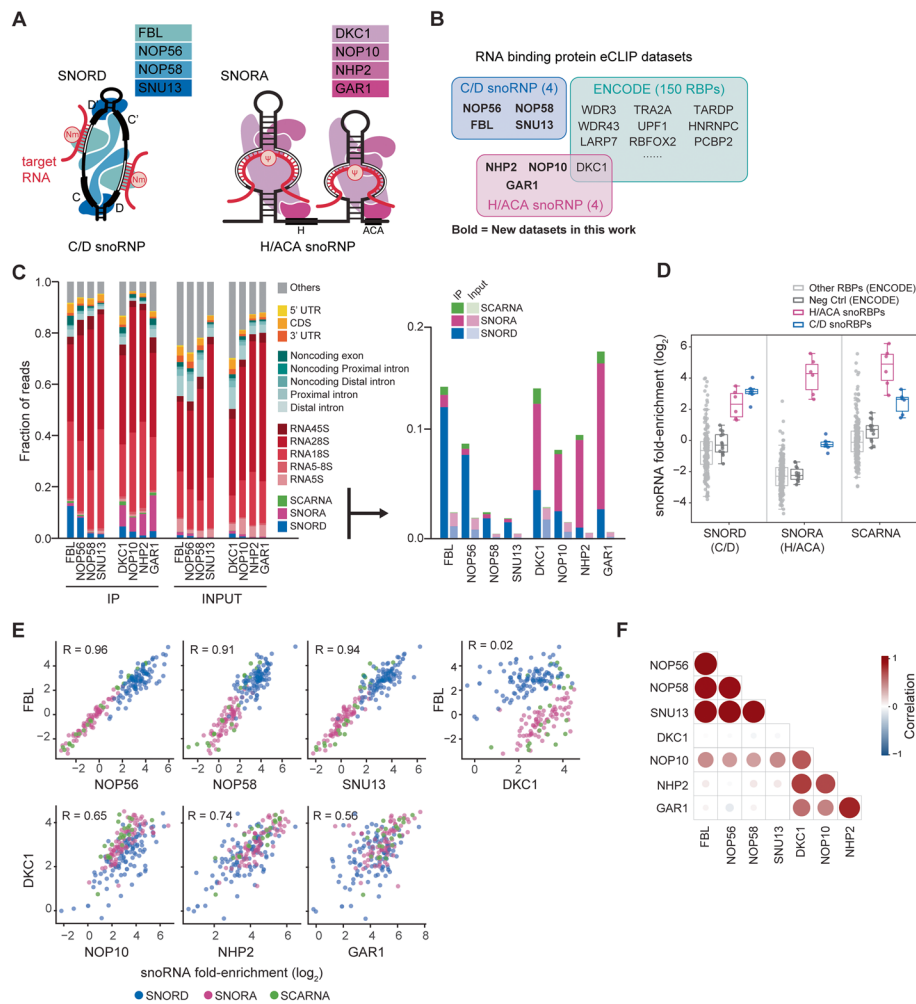


Fig. 1 Core snoRNP proteins show consistent RNA interactomes. **A** Schematic of (left) C/D and (right) H/ACA snoRNA-protein complexes. Red line represents the target RNA complementary to the snoRNA antisense element. **B** Overview of snoRNA-binding proteins with RNA interactomes profiled by ENCODE or (boldface) this work. **C** Distribution of reads to (left) major RNA classes and (right) snoRNA classes captured by eCLIP in K562 cells of the indicated core snoRBPs. **D** Fold-enrichment of different classes of snoRNAs in eCLIP datasets (both from ENCODE and generated in this study). Colors indicate different groups of protein baits (control—FLAG or V5). **E** Correlation of snoRNA fold-enrichment across (top) core C/D snoRBPs or (bottom) core H/ACA snoRBPs from eCLIP. Pearson correlations (R) are indicated (top left). Correlation between core C/D and H/ACA snoRBPs shown for contrast. Datapoints with less than 5 reads in IP were discarded. **F** Bubble plot showing pairwise correlation in snoRNA fold-enrichment between snoRBPs. Circle size and color indicate value of Pearson correlation coefficient (R). Data shown is average of 2 replicates per RBP

C/D, H/ACA, or hybrid (both) motifs, are involved in the biogenesis of spliceosomal RNAs (snRNAs). During their maturation, snoRNAs associate with core RNA-binding proteins (snoRBPs) to form functional snoRNPs. Specifically, C/D snoRNAs associate with FBL, NOP56, NOP58, and SNU13 (NHP2L1/15.5 K), while H/ACA snoRNAs associate with DKC1, NOP10, NHP2, and GAR1 (Fig. 1A). SnoRNPs translocate to the nucleolus or Cajal body, where they interact with nascent pre-rRNA or snRNA [1]. The antisense elements of snoRNAs engage in base pairing with their RNA targets, orchestrating the precise positioning of 2'-O-methylation (Nm) by C/D snoRNPs or isomerization of uridine to pseudouridine (Ψ) by H/ACA snoRNPs. Human rRNA contains more than 200 nucleotides that

undergo snoRNA-guided chemical modification [2]. Some of these chemical modifications cluster at functionally important regions of the ribosome, such as the peptidyl transferase center, tRNA binding sites, and the interface between the small and large subunits, and they contribute to the stabilization of rRNA folding, facilitation of efficient ribosome assembly, export of ribosomal subunits, and binding interactions with translation factors [3–5].

Over the years, research efforts have successfully identified snoRNA-target pairs for most known 2'-O-methylation and pseudouridine sites in rRNA. Advances in mass spectrometry approaches and high-throughput assays have facilitated the discernment of nucleotides subject to chemical modifications [2]. Additionally, bioinformatics tools have been employed to associate numerous snoRNAs with specific rRNA modification sites [6–9]. The development of RNA-RNA interaction mapping tools have validated additional snoRNA-rRNA interactions [10–15]. However, despite these collective efforts, the targets for a considerable subset of snoRNAs, known as orphan snoRNAs, have yet to be identified or experimentally validated.

Beyond their role in rRNA modifications, C/D snoRNAs can guide Nm in other RNA targets. This extends to snRNAs, tRNAs, and even a few mRNAs [13, 16–20]. Furthermore, C/D snoRNAs can act in a chaperone-like fashion independent of chemical modification. For instance, base pairing interactions between snoRNAs and pre-rRNA contribute to rRNA processing and assembly by influencing pre-rRNA conformation [21, 22]. Additionally, interactions between snoRNAs and pre-mRNA can contribute to splicing and 3' end processing [20, 23, 24], further highlighting the multifaceted roles of these snoRNAs beyond guiding chemical modifications. In many instances, these non-traditional functions require the assembly of additional proteins to snoRNA complexes [24–26]; however, the landscape of RNA-binding proteins (RBPs) and their snoRNA-interacting networks beyond the core snoRBP complexes remain undercharacterized.

Here we performed a deep, large-scale profiling of RNA interactions for all eight core RNA-binding protein components of the C/D and H/ACA snoRNA complexes. We then adopted chimeric eCLIP to directly capture snoRNA-target RNA interactions, utilizing both established core proteins and lesser-known snoRNA-associated RBPs as bait. Our results demonstrate that chimeric eCLIP successfully corroborated canonical snoRNA interactions with rRNAs and snRNAs. Moreover, we discovered novel interactions of orphan snoRNAs with rRNA and snRNA, a subset of which mediate chemical modification at the target site. Using non-core snoRNA-associated RBPs as baits in chimeric eCLIP revealed specific subnetworks of snoRNAs, suggesting specific roles of snoRNAs in distinct stages of snRNA or rRNA biogenesis. We further show that one such snoRNA, SNORD89, plays a key role in 2'-O-methylation of the G11 and G12 sites in U2 snRNA, which appears to be essential for maintaining imperfect splicing. Together, this study presents a systematic approach to investigate snoRNA-target interactions, revealing novel roles in RNA biogenesis and splicing regulation, and highlighting the potential for further discoveries in snoRNA biology.

Results

Core snoRNP proteins show consistent RNA interactomes

Previous profiling of the RNA interactomes of core C/D snoRNP proteins FBL, NOP56, and NOP58 by CLIP-seq led to the characterization of novel snoRNAs as well as the

identification of candidate interactions for orphan snoRNAs [27, 28]. However, of the four core H/ACA snoRNP proteins, the RNA interactome has only been profiled for DKC1 [27, 29]. To expand upon this prior work, we set out to use the updated eCLIP framework that allows deeper recovery of unique RNA molecules as well as quantitative normalization against input controls to comprehensively profile the direct interactions for the C/D and H/ACA snoRNP complex members [30]. We obtained and performed IP-western blot validation of antibodies against the four core proteins for both C/D (FBL, NOP56, NOP58, and SNU13) and H/ACA (DKC1, NOP10, NHP2, and GAR1) snoRNP complexes respectively (Fig. S1A), followed by eCLIP in K562 cells to facilitate contrast analysis with other ENCODE RBP datasets (Fig. 1B).

Basic analysis of snoRBP eCLIP indicated successful enrichment of snoRNAs (Fig. 1C,D). Similar to previous observations with PAR-CLIP [27], eCLIP for FBL, NOP56, NOP58, and SNU13 each showed significant enrichment for C/D snoRNAs versus paired input (≥ 6.5 -fold) (Fig. 1C). Over 5% of reads mapped to C/D snoRNAs for FBL and NOP56; NOP58 and SNU13 had significantly enriched but lower frequency of reads mapping to C/D snoRNAs ($> 1.5\%$) (Fig. 1C). The C/D snoRBPs showed an average 1.5-fold depletion for H/ACA snoRNAs compared to size-matched inputs, suggesting that the C/D complex shows specificity for binding to C/D snoRNAs (Fig. 1C,D). Similarly, all four H/ACA snoRBPs showed significant enrichment for H/ACA snoRNAs (≥ 6.2 -fold) (Fig. 1C,D). Over 5% of reads mapped to H/ACA snoRNAs for each RBP. Surprisingly, all four H/ACA snoRBPs also showed enrichment for C/D snoRNAs (≥ 2.5 -fold) (Fig. 1C,D), which may indicate a broader role for H/ACA snoRBPs or reflect low-level co-immunoprecipitation of FBL in these experiments (Fig. S1B). Seventy-seven percent of reads in C/D snoRBP and 68% in H/ACA snoRBP eCLIP mapped to either precursor or mature rRNA (Fig. 1C), a significant enrichment over either all RBPs profiled by ENCODE or even the subset of nucleolar and rRNA-associated RBPs in ENCODE (Fig. S1C), consistent with snoRBPs directly interacting with rRNA during rRNA biogenesis. In contrast, pre-mRNA and mRNA regions were predominantly depleted (Fig. S1C).

Previous research has observed examples of sub-complex specificity, as SNU13 is involved in other RNA-protein complexes such as the U4/U6.U5 tri-snRNP [31] in addition to its role in snoRNP assembly. Consistent with this, eCLIP of SNU13 but not the other C/D snoRBPs showed enrichment at the 5' stem loop of the U4 snRNA similar to other U4-interacting tri-snRNP factors (Fig. S1D). However, when we performed transcriptome-wide analysis comparing the enrichment of individual snoRNAs, we observed striking pair-wise correlation in per-snoRNA enrichment among all core C/D snoRBPs (all Pearson $R > 0.90$) and significant correlation in enrichment among all core H/ACA snoRBPs ($R > 0.50$) (Fig. 1E,F), which was independent of FBL or DKC1 co-immunoprecipitation (Fig. S1B). In contrast, there is little correlation in per-snoRNA enrichment between C/D and H/ACA snoRBPs, such as FBL and DKC1 ($R = 0.02$) (Fig. 1E,F). To consider these results in the context of outgroup (non-snoRNA-related) RBPs, we utilized available ENCODE eCLIP data to compare the correlation of enrichment for individual snoRNAs across 149 other RBPs. Although the majority of RBP and negative control (using FLAG or V5 pulldown in wildtype cells) datasets were depleted for snoRNAs (Fig. 1D), we surprisingly observed a significant per-snoRNA correlation with FBL

across RBP datasets (median $R=0.62$) and negative controls (median $R=0.76$) that may reflect low-level co-precipitation of the C/D snoRNP complex across eCLIP experiments (Fig. S1B,E). However, the correlation between pairs of core C/D or H/ACA snoRBPs was higher than with nearly any other RBPs (Fig. S1E), providing further evidence that the four core C/D and four core H/ACA snoRBPs coordinately associate with C/D and H/ACA snoRNAs, respectively, in a consistent manner.

In order to examine how snoRBP interaction profiles compare across cell types, we performed FBL and DKC1 eCLIP in 293T and HepG2 cells in addition to K562 cells. The enrichment of snoRNAs across the profiled cell lines is highly correlated (Fig. S1F). When considering well expressed snoRNAs present at more than 10 reads per million in at least one cell type, only 6 snoRNAs (SNORD50, SNORD64, SNORD109, SNORD115, SNORD116, and SNORA35) showed cell type-specific binding to FBL or DKC1 (Fig. S1G). This likely reflects the cell type-specific expression of these snoRNAs. These data suggest that the snoRNA landscape is highly consistent across cancer cell types. In summary, we comprehensively profiled the RNA interactions of all core proteins in both the C/D and H/ACA snoRNP complexes. We demonstrated that the core proteins within each complex coordinately associate with the respective C/D or H/ACA snoRNAs and that the binding specificity of snoRNP complexes is strongly cell type independent.

Chimeric eCLIP of core C/D snoRNP proteins comprehensively recovers known C/D snoRNA interactions

Chimeric CLIP approaches enable unambiguous identification of RNA-RNA interactions by taking advantage of an intramolecular ligation of interacting RNAs during immunoprecipitation, which can then be read out as a ‘chimeric’ sequencing read that contains both fragments [15]. Prior analysis of CLIP for C/D snoRBPs successfully recovered C/D snoRNA-target interactions through mapping chimeric reads [14, 15, 28]. Here, we set out to determine whether we could deeply interrogate snoRNA-target interactions across cell lines and organisms with chimeric eCLIP, using core C/D snoRNP proteins as bait (Fig. 2A). Chimeric eCLIP combines the library preparation optimizations in eCLIP with an additional ligation step to encourage intermolecular ligations between co-precipitated RNA-target fragments [32]. SnoRNA targets have been extensively queried in human cancer cell lines but less characterized in rare cell types or other mammalian systems, so we profiled mouse embryonic stem cells (mESC) in addition to a standard human cell line (293T) and implemented a computational pipeline to identify snoRNA:target chimeric reads (Fig. S2A).

Chimeric eCLIP generated 0.2–0.6% chimeric reads out of total reads in FBL and NOP56 libraries from mESC and FBL, NOP56, and NOP58 libraries from 293T cells (Fig. S2B). This rate of chimeric reads is similar to the 0.1–1.5% observed from prior CLASH and SPLASH approaches in human cells [11, 14, 28], and our recovery of 0.2–0.4% snoRNA:rRNA chimeras out of all sequenced reads is improved upon the 0.02% or less observed in prior studies [14, 18, 28]. The per-snoRNA abundance was highly correlated between non-chimeric and chimeric reads (Fig. 2B), indicating that chimeric ligation does not cause biased recovery of snoRNAs. The number of chimeric reads per snoRNA was highly correlated between different core C/D snoRBP baits in both mESC (Fig. 2C) and 293T cells (Fig. S2C). This result, similar to our observations by eCLIP,

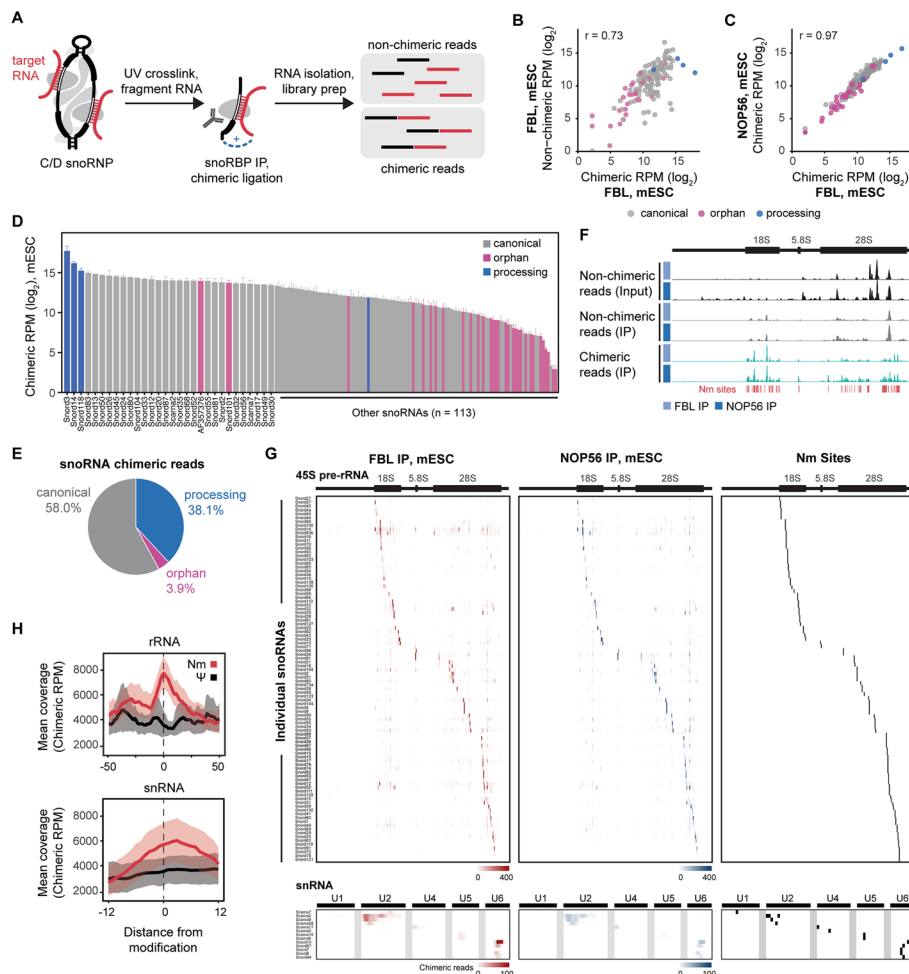


Fig. 2 Chimeric eCLIP of core C/D snoRNP proteins comprehensively recovers known C/D snoRNA interactions. **A** Schematic of chimeric eCLIP procedure. **B** Correlation of non-chimeric versus chimeric snoRNA read abundance from FBL chimeric eCLIP in mouse embryonic stem cells (mESC). Pearson correlation (R) is indicated. **C** Correlation of snoRNA chimeric read abundance from FBL versus NOP56 chimeric eCLIP in mESC. Pearson correlation (R) is indicated. **D** Chimeric read abundance for individual snoRNAs colored according to snoRNA functional class. The y-axis indicates average of chimeric RPM in FBL and NOP56 chimeric eCLIP. **E** Pie chart of total number of snoRNA chimeric reads from mESC according to snoRNA functional class from FBL chimeric eCLIP. **F** Browser tracks of non-chimeric reads and snoRNA chimeric reads mapped to pre-rRNA as captured by FBL and NOP56 chimeric eCLIP in mESC. Annotated Nm sites are shown. **G** Heatmap of chimeric read coverage across pre-rRNA and snRNA from FBL and NOP56 chimeric eCLIP for canonical snoRNAs. Known Nm target sites are shown in black. **H** Metagene plots of mESC chimeric read coverage flanking Nm (red) and pseudouridine (black) sites in rRNA and snRNA. Chimeric RPM, reads per million chimeric reads. Data shown is from 1 replicate per RBP

suggests a consistent recovery of snoRNA-target interactions using any of the core C/D snoRBPs. It is noteworthy that the number of chimeric reads between core C/D snoRBPs was highly correlated for SNORD13, an acetylation-guiding C/D snoRNA, as well as orphan C/D snoRNAs that lack known targets (Fig. 2C, S2C). These results implicate FBL as a constitutive component of the C/D snoRNP complex irrespective of Nm-guiding activities, and they further justify the suitability of FBL chimeric eCLIP approaches for identifying targets of orphan snoRNAs.

We captured chimeric reads for nearly all expressed C/D snoRNAs in each cell line, namely 143 out of 144 (99%) expressed snoRNAs in mESC [$\text{RPM} \geq 3$] (Fig. 2D) and 116 out of 118 (98%) expressed snoRNAs in 293 T cells [$\text{RPM} \geq 3$] (Fig. S2D). The capture of chimeric reads to a larger proportion of snoRNAs in mESC compared to 293T cells was likely due to the greater sequence depth of the mESC libraries (Fig. S2B; 80 M raw reads in mESC versus 30 M raw reads in 293T). The highest numbers of chimeric reads were captured for highly abundant snoRNAs that mediate pre-rRNA processing, such as Snord3, Snord14, and Snord118, but we observed substantial coverage for both “canonical” snoRNAs, which guide modification on rRNA and snRNA, and orphan snoRNAs whose targets are unknown (Fig. 2D,E, S2D). The few snoRNAs for which chimeric reads were not captured were lowly expressed.

As an initial evaluation of the success of chimeric eCLIP in identifying known C/D snoRNA-target interactions, we mapped chimeric reads to pre-rRNA and snRNA. Chimeric reads were observed primarily to the mature regions of rRNA and had a distinct distribution profile compared to non-chimeric reads from input or IP samples (Fig. 2F). Visual examination of individual snoRNA:rRNA and snoRNA:snRNA chimeric read tracks showed a marked enrichment of chimeric reads at their known Nm-guiding target sites in mESC (Fig. 2G) and 293T cells (Fig. S2E). Furthermore, metagene analysis highlighted a significant enrichment of chimeric reads at Nm sites in both rRNA and snRNA that is not observed at pseudouridylation sites (Fig. 2H, S2F). All together, these analyses lend strong support to the power and accuracy of chimeric eCLIP in experimentally detecting snoRNA-target interactions by C/D snoRBPs.

Transcriptomic mapping of C/D snoRNA chimeras calls novel, high-confidence interactions

Next, we performed transcriptome-wide mapping of the chimeric reads obtained from core C/D snoRBP chimeric eCLIP in mESC and 293 T cells. We examined the chimeric read distribution among different RNA classes. The majority of snoRNA chimeras mapped to rRNA (~75%, mESC; ~55%, 293T) and, to a lesser extent, pre-mRNA (~10%, mESC; ~20%, 293T), snRNA (~0.3%, mESC and 293T), and tRNA (~0.1%, mESC; ~0.4%, 293T) (Fig. 3A, S3A). When the chimeric read distribution was analyzed for individual canonical snoRNAs, we observed that rRNA-targeting snoRNAs had the highest proportion of rRNA-mapping chimeras, whereas some snRNA-targeting snoRNAs had an appreciably higher proportion of snRNA-mapping chimeras (Fig. S3B). Interestingly, the chimeric read distribution for individual orphan snoRNAs hinted at possible target classes; Snord23 and Snord89 chimeras were enriched for snRNAs while Snord90 and Snord101 were enriched for rRNA (Fig. S3B).

To call high-confidence interaction sites across the transcriptome, we performed peak calling using Clipper [33]. Peaks at known interaction sites were readily distinguished from poorly supported “background” peaks when two parameters were considered: peak fold enrichment (chimeric reads from snoRBP IP relative to non-chimeric reads from input) and fraction of per-snoRNA reads in peak (chimeric reads in peak relative to total number of per-snoRNA chimeric reads) (Fig. S3C). The latter identifies the most predominant peak(s) for each snoRNA. In order to evaluate the utility of using peak fraction as a parameter to call true interactions, we generated a receiver-operating characteristic curve (ROC) based on peaks for snoRNAs known to guide Nm on rRNA. To generate

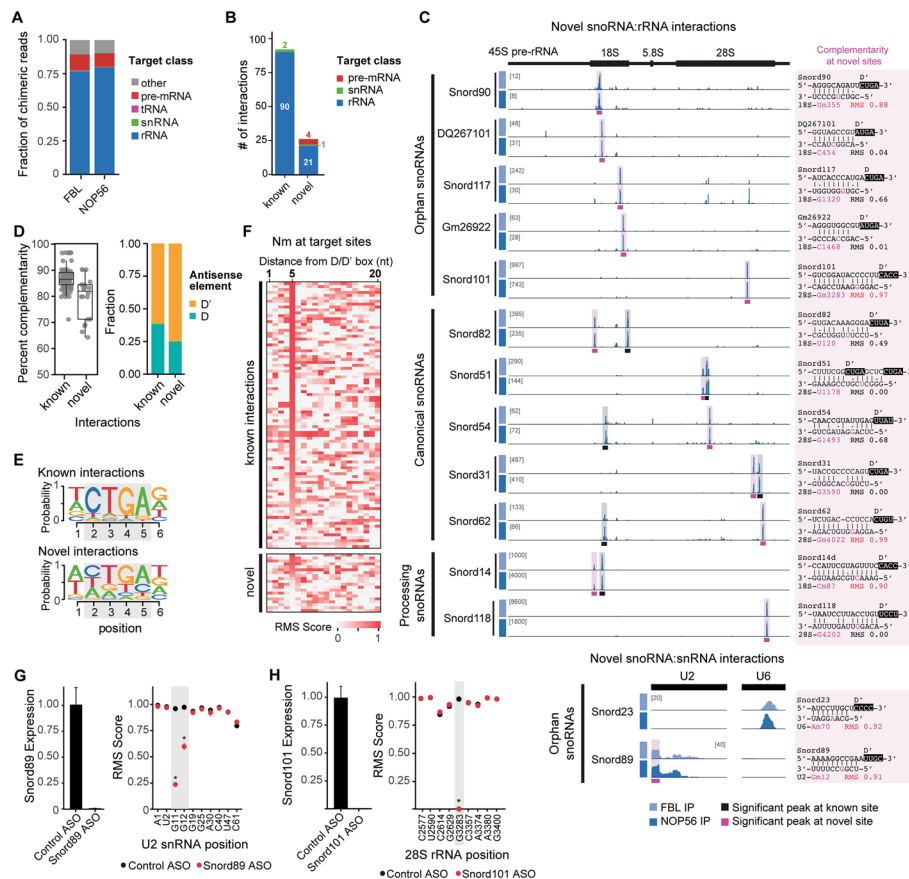


Fig. 3 Transcriptomic mapping of C/D snoRNA chimeras calls novel, high-confidence interactions in mESCs. **A** Stacked bars indicate the fraction of C/D snoRNA chimeric reads mapping to distinct classes of possible target RNAs from FBL and NOP56 chimeric eCLIP. **B** Number of high-confidence snoRNA-target interactions identified by chimeric eCLIP according to interaction status and target class. **C** Browser tracks of snoRNA chimeric reads mapped to pre-rRNA or snRNA as captured by FBL and NOP56 chimeric eCLIP from mESC. Significant peaks at (black) known or (pink) novel sites. (Right) Base pair complementarity of novel interactions. Ribometh-seq (RMS) score is shown for the 5th nucleotide from the D/D' box when high methylation is observed. **D** (Left) Percent complementarity of base pairing in snoRNA-target interactions for significant peaks at known or novel sites and (right) fraction of interactions associated with D or D' antisense elements. **E** Consensus sequence of the D or D' box predicted to guide the known or novel snoRNA-target interactions. **F** RMS score at rRNA or snRNA target sites for known versus novel interactions. The 5th nucleotide is the expected position for methylation. (RMS scores are average of 2 biological replicates). **G** (Left) Snord89 expression following treatment with non-targeting (control) or Snord89-targeting ASO and (right) RMS scores at methylated nucleotides in U2 snRNA. * indicates $P < 0.05$, two-tailed unpaired Welch's t -test. $N = 2$ replicates per condition. **H** (Left) Snord101 expression following treatment with non-targeting (control) or Snord101-targeting ASO and (right) RMS scores at methylated nucleotides in 28S rRNA. * indicates $P < 0.05$, two-tailed unpaired Welch's t -test. $N = 2$ replicates per condition

the curve, peaks overlapping known Nm target sites were considered true positives and peaks at unannotated sites were considered false positives. The ROC for peaks in known rRNA-targeting snoRNAs yielded an area under the curve (AUC) of 99.2% in mESCs and 97.4% in 293T cells (Fig. S3D), indicating that the model has a high probability of correctly distinguishing true positives from false positives. The optimal threshold for peak fraction as determined by ROC analysis was 0.026 in mESC and 0.075 in 293T cells. These thresholds resulted in >93% sensitivity (i.e., high true positive rate) and >93% specificity (i.e., low false positive rate). To further minimize the false positive

rate and stringently call high-confidence interactions, we selected thresholds of peak fraction > 0.1 and peak fold enrichment > 3 for subsequent analyses.

We called a maximum of two significant peaks per snoRNA (Fig. S3E), consistent with the presence of two antisense elements per snoRNA. When considering significant peaks called in both FBL and NOP56 chimeric eCLIP datasets from mESCs (i.e., reproducible peaks), we identified high-confidence interactions for 70% (102 out of 145) of expressed snoRNAs. This included significant peaks at 84% (90 out of 107) of known snoRNA-rRNA interactions and two known snoRNA-snRNA interactions (Fig. 3B). Peaks were present at an additional 17 known rRNA and snRNA interaction sites but fell below the stringent thresholds (Fig. S3F). In 293T cells, we called a smaller percentage of snoRNA-rRNA interactions that are annotated in snoDB (Fig. S3E,G), a database of human snoRNA interactions that includes non-canonical interactions from RNA-RNA interactome mapping studies.

Importantly, our analyses detected significant, reproducible peaks at a number of novel snoRNA interaction sites (Additional file 2: Table S1). This included 21 novel snoRNA-rRNA and 1 novel snoRNA-snRNA interactions in mESC (Fig. 3B). While an additional 4 novel interactions were observed with pre-mRNA, the peaks were located around or adjacent to intron-embedded snoRNAs (Fig. S3H), potentially indicating spurious chimeric RNA formation during snoRNA biogenesis or incomplete snoRNA annotation. Expanded analysis of genomic peaks without any cutoffs similarly indicated limited peaks outside of such artifacts (Fig. S3I), with the majority of peaks in introns or non-coding exons, suggesting that many of the pre-mRNA chimeric reads we observe are sporadically dispersed throughout the genome and may not reflect strong interactions. In total, we assigned high-confidence interactions for 10 orphan snoRNAs (Additional file 2: Table S1); for example, Snord89 with U2 snRNA and Snord90, Snord101, Snord117, DQ267101, and Gm26922 with rRNA (Fig. 3C). We also observed an interaction between orphan Snord23 and U6 snRNA, but it fell below the significance cutoff (Fig. 3C). Beyond orphan snoRNAs, we called novel interactions for canonical snoRNAs that already have one antisense element assigned as an Nm guide. For example, Snord31, Snord51, Snord54, Snord62, and Snord82 each had two significant peaks in rRNA (Fig. 3C) — one peak at the known Nm target site and a second peak at the novel site. Lastly, we detected significant, reproducible peaks for two snoRNAs that mediate pre-rRNA processing, Snord14 and Snord118 (Fig. 3C). A high degree of concordance was observed across reproducible peaks in mESC and 293T cells (Additional file 2: Table S1).

Box C/D snoRNAs base pair with their targets through an antisense element located immediately upstream of the D or D' box element. To further characterize the interactions identified by chimeric eCLIP, we predicted the snoRNA antisense element associated with each interaction, then quantified the base pair complementarity of the snoRNA-target interaction (Methods). The base pair complementarity for novel snoRNA-rRNA interaction sites was slightly lower than known sites (78.1% mean identity at novel sites versus 86.8% at known sites) and was more commonly associated with D' box elements (Fig. 3D). The strength of the conserved "CTGA" box motif was higher for known snoRNA-rRNA interactions compared to novel interactions (Fig. 3E), which is consistent with the lower conservation of D' box motifs compared to D box motifs. This observation suggests that the novel interactions identified by chimeric eCLIP more

frequently involve less conserved D' box motifs, which could explain why these interactions have not been identified by previous bioinformatic approaches utilizing sequence complementarity modeling.

Canonical snoRNAs guide Nm to the site on target RNA that is base paired exactly 5 nucleotides upstream of the snoRNA D/D' box. To determine potential snoRNA-guided methylation at novel interactions in mESC, we quantified Nm levels in rRNA and snRNA by RiboMeth-seq (RMS) [34]. High levels of methylation were observed at the fifth nucleotide position for nearly all known snoRNA interactions detected in our study (mean RMS=0.78, Fig. 3F). Novel interactions displayed overall lower RMS scores at the predicted methylation sites (mean RMS=0.34, Fig. 3F), indicating possible methylation-independent functions of these interactions. Several novel sites, though, did display high levels of methylation at the expected nucleotide, including 18S-C87 (Snord14), 18S-U355 (Snord90), 28S-G3283 (Snord101), 28S-G4022 (Snord62), U2-G12 (Snord89), and U6-A70 (Snord23) (Fig. 3C). Snord60 is already assigned as the guide for modification at 28S-G4022, so the co-detection of Snord60 and Snord62 at this site in our study could indicate compensatory or competitive interactions that merit further investigation.

Based on our data we hypothesized that Snord89 guides methylation at U2-G12, as similarly observed in a yeast cell system [35]. To examine the targeting specificity of Snord89 in mouse cells, we performed loss-of-function experiments using gapmer antisense oligonucleotides (ASOs) supportive of RNase H recruitment. Surprisingly, we found that ASO-mediated knockdown of Snord89 resulted in loss of methylation at two neighboring nucleotides in U2. Methylation at U2-G11 and U2-G12 were decreased by 72 and 37%, respectively (Fig. 3G). We then validated the targeting specificity of Snord101 using the same approach. ASO-mediated knockdown of Snord101 resulted in complete loss of methylation at 28S-G3283 with no effect on the flanking Nm sites (Fig. 3H).

We also tested whether the chimeric eCLIP approach could capture H/ACA snoRNA-target interactions by performing chimeric eCLIP with DKC1 and GAR1 as the bait proteins from 293T cells. Analysis of non-chimeric reads from chimeric eCLIP yielded similar results to standard eCLIP, as over 24% of reads mapped to snoRNAs with greater recovery for H/ACA snoRNAs (16 and 20% of total reads by DKC1 and GAR1) versus C/D snoRNAs (7% in both RBPs) (Fig. S4A). Chimeric analysis recovered ~1% chimeric reads out of total reads, but despite the higher recovery of H/ACA snoRNAs among non-chimeric reads, we observed that less than half of the chimeric reads contained an H/ACA snoRNA (Fig. S4B). Manual inspection of well-studied H/ACA snoRNAs suggested that while some known sites may be captured, most showed poor recovery and resolution at known target regions (Fig. S4C). Performing peak calling confirmed that DKC1 chimeric eCLIP had at best marginal recovery of true interactions (Fig. S4D). We hypothesize that the distinct structural complexity of H/ACA snoRNAs may make them refractory to standard chimeric CLIP approaches and that alternative approaches will be required to profile H/ACA interactomes.

Thus, these results confirm that chimeric eCLIP can be used to find new C/D snoRNA interactions but requires further optimization for H/ACA snoRNAs. We identified high-confidence interactions with reproducibility between different core C/D snoRBP baits in rRNA and snRNA, a subset of which may involve alternative functions or regulatory

mechanisms beyond 2'-O-methylation. Compared to bioinformatic approaches, this experimental approach is agnostic to the identification of D/D' box motifs, target RNA class, or presence of chemical modification at the target site.

Identification of specific subsets of snoRNA-target interactions using orthogonal protein baits

In addition to the core C/D and H/ACA snoRNA-binding proteins, several additional RBPs have been reported to associate with snoRNAs and regulate their functions beyond guiding rRNA modifications [24, 36]. As these interactions are under-explored, we set out to test whether performing chimeric eCLIP with less-studied snoRNA-associated proteins would enrich for functionally related subsets of snoRNAs and help uncover new aspects of snoRNA biology. We first identified candidate bait proteins to use in our study by integrating our core C/D and H/ACA snoRBP eCLIP datasets with the 150 RBPs profiled by ENCODE to analyze snoRNA enrichment with a customized analysis pipeline [29, 37]. While the majority of evaluated RBPs displayed a depletion for both C/D and H/ACA snoRNAs, 11 RBPs (in addition to the core snoRBPs above) showed at least fourfold enrichment for snoRNAs and may represent potential snoRNA partners (Fig. 4A). These non-core snoRBPs clustered into two functional annotations: a cluster of RBPs that included splicing- and spliceosomal RNA-associated factors (LARP7, NOLC1, PTBP1, SMNDC1, TRA2A, and ZC3H8), discussed further below, and a cluster of rRNA processing factors (AATE, UTP3, UTP18, WDR3, WDR43) which showed even stronger specificity for C/D snoRNAs than the core C/D snoRBPs (Fig. 4A). Considering individual snoRNA enrichment, we observed that these rRNA processing RBPs, members of the small-subunit (SSU) processome [38, 39], were particularly enriched for the processing snoRNA SNORD3 (U3) relative to FBL (Fig. 4B, S5A). SNORD3 contains an extended 5' domain that interacts with pre-rRNA and contributes to ribosomal RNA processing [40, 41], which makes it notably structurally distinct from other C/D-box snoRNAs that direct methylation through antisense elements (upper D/D' box) and may explain why SSU processome factors show stronger SNORD3 enrichment than core snoRNP proteins. Comparing SNORD3 fold-enrichment across all RBPs in ENCODE confirmed that rRNA processing RBPs, and particularly the small-subunit processome, showed strong enrichment for SNORD3 (Fig. 4C, S5B), consistent with the critical role of SNORD3 in coordinating the function of the SSU in rRNA processing [42, 43].

To test whether we could recover distinct interaction profiles of SNORD3 associated with these SSU factors versus the core C/D snoRNP complex, we performed chimeric eCLIP for WDR43 and UTP18 in K562 cells (Fig. S5C). Although SNORD3 was typically the most frequently observed snoRNA in chimeric reads for all RBPs profiled (Fig. S5D), WDR43 and UTP18 showed an even higher frequency of SNORD3:rRNA chimeras compared to FBL, NOP56, or NOP58 (Fig. S5E). Visual examination of SNORD3:rRNA chimeric read tracks showed a strong enrichment of SNORD3 chimeric reads in the 5'ETS and 18S regions of pre-rRNA, with a distinct interaction profile for UTP18 and WDR43 compared to FBL or other core C/D snoRBPs (Fig. 4D). In WDR43 and UTP18 pulldown compared to FBL, SNORD3 chimeric reads were enriched and preferentially positioned at previously identified U3 interaction sites at the 01, A0, and A1 loci within the 5'ETS and a loci at ~4800 nt in the 18S rRNA (Fig. 4D,E, S5E, purple, orange, yellow, and green

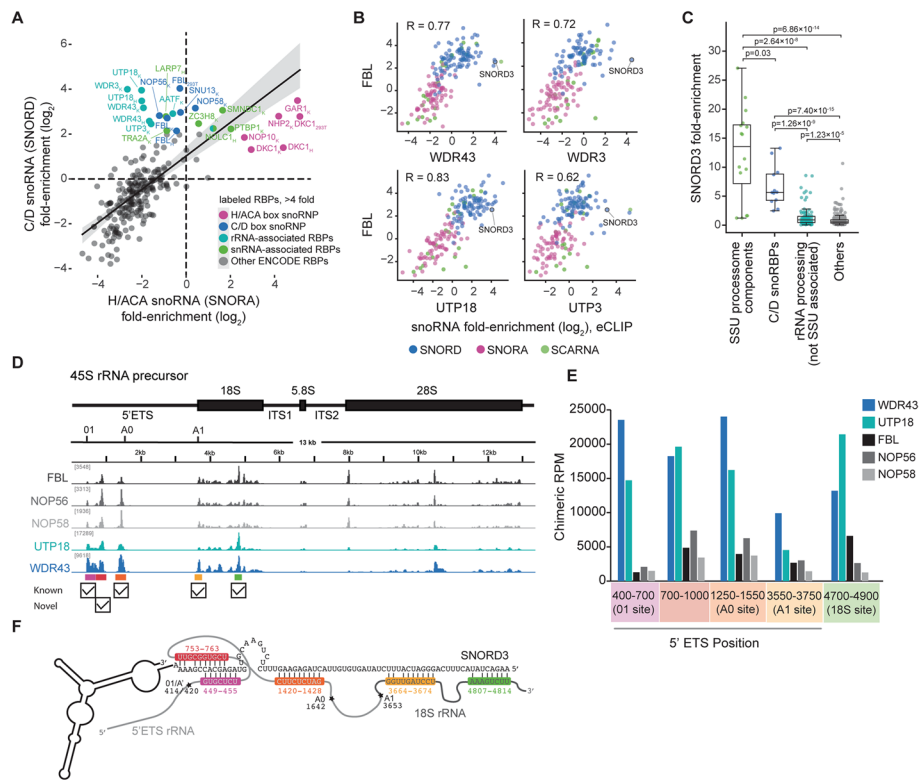


Fig. 4 RBPs that function in ribosomal RNA processing recover unique SNORD3 chimeric reads. **A** Fold-enrichment correlation between (x-axis) H/ACA and (y-axis) C/D snoRNAs across 8 snoRBPs and 223 ENCODE eCLIP datasets. **B** Correlation of snoRNA fold-enrichment in FBL and ribosomal RNA-associated RBP eCLIP in K562 cells. Correlation (R) is shown. Only snoRNAs with 5 or more reads in IP were plotted. **C** Box plot showing fold-enrichment of SNORD3 in eCLIP datasets for indicated groups of RBPs. Two-sample Kolmogorov–Smirnov (KS) test was performed. **D** Browser tracks of SNORD3 chimeric reads mapped to pre-rRNA as captured by chimeric eCLIP for the indicated RBPs in 293 T (FBL, NOP56, NOP58) or K562 (UTP18, WDR43) cells. Check marks indicate the known interactions or novel interactions identified in our study. **E** Bars indicate the abundance of SNORD3 chimeric reads (Reads Per Million Chimeric reads) at different processing sites in the pre-rRNA across the indicated RBPs. **F** Schematic of predicted structures of potential SNORD3-rRNA interactions, with labelled regions colored according to **D**. eCLIP data shown is average of 2 replicates per RBP; chimeric eCLIP results shown are a single replicate per RBP

peaks), consistent with well-established SSU-associated SNORD3 roles in ribosomal processing [42, 44, 45]. Notably, we also observed a novel U3 interaction in the region between the 01 and A0 sites (700–1000 nt) on rRNA (Fig. 4D,E, S5F, red peak). Sequence alignment indicates that sequences within the 01 (400–700 nucleotide) and intermediate 700–1000 nucleotide regions of pre-rRNA are complementary to overlapping regions of SNORD3 (Fig. 4F), suggesting that the chimeras may reflect sequential interactions during the complex series of processing steps involved in pre-rRNA transcription, folding, and maturation [46]. Overall, these results indicate that chimeric eCLIP for SSU processing components can recover SNORD3 interactions distinct from those observed with FBL, validating the principle that using unique protein baits can reveal new snoRNA interaction landscapes.

Chimeric eCLIP of LARP7 and NOLC1 detects unique snoRNA-snrRNA interactions

Post-transcriptional modifications of snRNAs are essential for spliceosomal fidelity and are largely guided by snoRNAs, with the scaRNA class playing a particularly important role [47, 48]. More snoRNA-snrRNA interactions continue to be discovered, including our identification of Snord23-U6 and Snord89-U2 interactions above and other recent work [18]. This, together with a recent study that identified LARP7 as a novel bridging factor for snoRNA-guided modifications on U6 [25, 49], suggests that more principles of snRNA regulation by snoRNAs are yet to be uncovered. As such, we next asked whether chimeric profiling of the splicing- and spliceosomal RNA-associated proteins we identified above could enrich for unique snoRNA-snrRNA regulatory networks.

As validation of this approach, we first examined LARP7. Previous studies proposed a mechanism in which LARP7 binds the subset of C/D snoRNAs that have been shown to guide U6 2'-O-methylation, including SNORD7, SNORD8, SNORD9, SNORD10, SNORD67, and SNORD94 [25, 49]. Consequently, we performed chimeric eCLIP on LARP7 and FBL in HepG2 cells (Fig. S6A) to determine if LARP7 could capture and enrich for these snoRNA-U6 interactions. We observed that the previously characterized LARP7-associated snoRNAs had the highest enrichment among non-chimeric (i.e., snoRNA only) and chimeric reads in LARP7 compared to FBL chimeric eCLIP (Fig. 5A, B, S6B). SnoRNA:U6 chimeras were recovered for five of the six LARP7-associated snoRNAs, and these chimeras mapped to the known U6 Nm target sites in both FBL and LARP7 datasets (Fig. 5C,D), validating the role of LARP7 in bridging functional snoRNA-snrRNA interactions. Many of the other U6-interacting snoRNAs annotated in snoDB were not captured by FBL, and manual inspection of their annotation source found these were often supported by sparse interaction data and lacked validation of snoRNA-responsive methylation. Overall, recovery of chimeras for known snoRNA-U6 interactions was 2.2 times higher in LARP7 versus FBL chimeric eCLIP, whereas recovery of chimeras for known snoRNA-rRNA interactions was dramatically lower (11.9 times) (Fig. 5E, F). These data confirm that chimeric eCLIP can capture and enrich for specific subsets of snoRNA interactions involving LARP7.

We then looked for novel RBP baits that could highlight additional snoRNA-snrRNA interaction principles. We further analyzed the ENCODE RBP eCLIP data and identified four spliceosomal RNA-associated proteins (NOLC1, SMNDC1, ZC3H8, and PTBP1) with co-enrichment for both snoRNAs and scaRNAs (Fig. S6C). These RBPs were also often enriched for either U2 or U6 snRNAs, echoing their known roles in snRNA processing (Fig. S6D,E) [50–53]. Next, we performed chimeric eCLIP for NOLC1, SMNDC1, and ZC3H8 in the same cell lines as the ENCODE eCLIP experiments: NOLC1 in HepG2 cells and SMNDC1 and ZC3H8 in K562 cells (Fig. S6A). Due to technical issues, PTBP1 was not profiled. We noted that the size-resolved band of NOLC1 was present in standard eCLIP but lost after chimeric ligation (Fig. S6A,F), suggesting that this ligation may create a mixture of higher-order complexes.

Although rRNA chimeras still account for the highest percentage of total chimeras (Fig. S6G), NOLC1 chimeric eCLIP showed particular enrichment for snoRNA:snRNA chimeras compared to either FBL or LARP7, with a pronounced enrichment for both U2 and U6 chimeras (Fig. 5G). In contrast, SMNDC1 and ZC3H8 had low recovery of snoRNA:snRNA chimeras for U2 and U6 despite their enrichment among non-chimeric

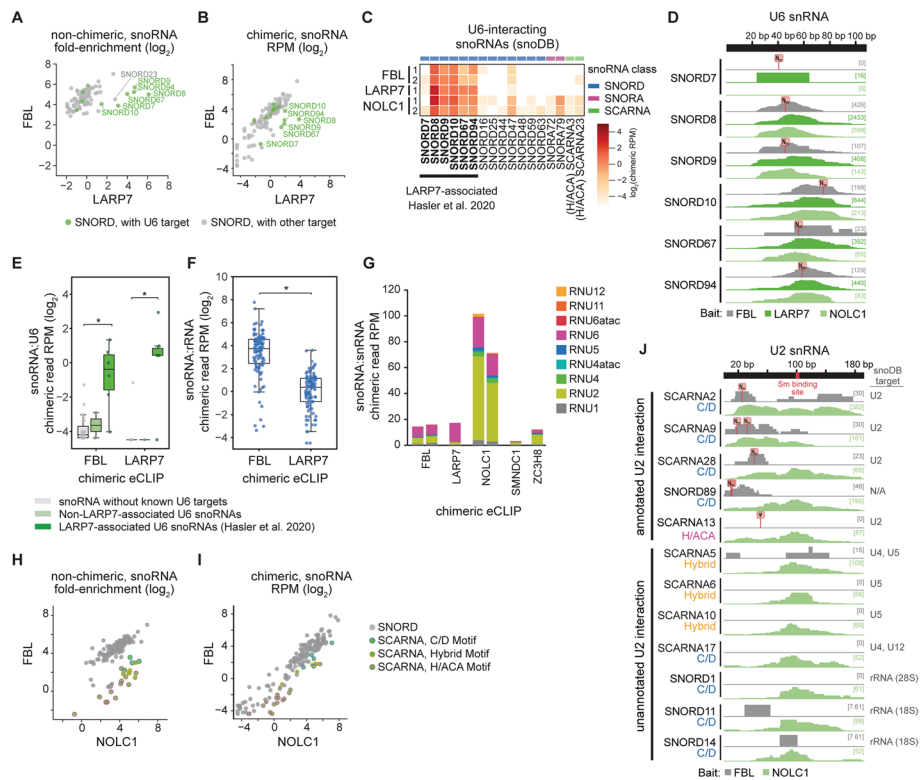


Fig. 5 Chimeric eCLIP for spliceosomal RNA-associated RBPs enrich for snoRNA-snoRNA interactions. **A** Fold-enrichment of non-chimeric C/D snoRNA reads from FBL versus LARP7 chimeric eCLIP in HepG2 cells. Datapoints for C/D snoRNAs with U6 interactions annotated in snoDB are colored. Datapoints with < 5 IP reads were discarded. **B** C/D box snoRNA chimeric read abundance (RPM) from FBL versus LARP7 chimeric eCLIP. Datapoints for C/D snoRNAs with U6 interactions annotated in snoDB are colored. **C** Heatmap of snoRNA chimeric read abundance (RPM) from FBL, LARP7, and NOLC1 chimeric eCLIP replicates for all snoRNAs with annotated U6 interactions. **D** Browser tracks show read density (per million chimeric reads) for U6-interacting snoRNA chimeras along the U6 snRNA for a single representative replicate. **E** SnoRNA:U6 chimeric read abundance (RPM) from FBL or LARP7 chimeric eCLIP. Colors indicate snoRNAs classified as (green) LARP7-associated U6 snoRNAs, (light green) non-LARP7-associated U6 snoRNAs, and (gray) all other snoRNAs. * indicates $P < 0.05$, unpaired two sample t -test. **F** SnoRNA:rRNA chimeric read abundance (RPM) for snoRNAs with known rRNA target sites from FBL or LARP7 chimeric eCLIP. * indicates $P < 0.05$, unpaired two-sample t -test. **G** Target distribution of snoRNA:snRNA chimeric reads (RPM) recovered in chimeric eCLIP for the indicated RBPs. **H** Fold-enrichment of non-chimeric snoRNA reads in FBL versus NOLC1 chimeric eCLIP in HepG2 cells. Datapoints with < 5 IP reads were discarded. Circle outline color represents the type of SCARNA with (blue) C/D box motif, including Tandem-C/D SCARNAs, (pink) H/ACA box motif, including Tandem-H/ACA SCARNAs, and (orange) hybrid SCARNAs that possess both C/D and H/ACA box motifs. **I** SnoRNA chimeric read abundance (RPM) in FBL versus NOLC1 chimeric eCLIP. **J** Browser tracks show read density (per million chimeric reads) for snoRNA:U2 chimeric reads along the U2 snRNA for known and candidate U2-interacting snoRNAs for a single representative replicate (see Fig. S6L for second replicate). RPM: reads per million sequenced reads. Unless otherwise indicated, data shown is average of two replicates (FBL, NOLC1) or a single replicate (LARP7)

reads (Fig. 5G, S6H), and we did not pursue further analysis on these RBPs. Unlike LARP7, NOLC1 chimeric eCLIP did not enrich for a specific subset of C/D snoRNAs; rather, the entire class of scaRNAs was enriched in NOLC1 versus FBL chimeric eCLIP among both non-chimeric reads (Fig. 5H) as well as chimeric reads (Fig. 5I). This included not only scaRNAs containing box C/D motifs, but also H/ACA and hybrid motifs, consistent with the role of NOLC1 in maturation and function of both snoRNA

classes [54]. NOLC1 replicates exhibited high consistency in snoRNA fold enrichment and chimeric read frequency (Fig. S6I).

For C/D-containing snoRNAs known to target U2 or U6, in many cases NOLC1 recovered chimeras at their known target sites, as illustrated for SCARNA2 and SCARNA9 in U2 (Fig. 5J) and SNORD8, SNORD9, and SNORD10 in U6 (Fig. 5D). The enrichment profiles for these known snoRNA guides were very similar to chimeric eCLIP of FBL (Fig. 5D, I), suggesting NOLC1 may act in concert with the core snoRNP at these target sites. In addition, we also reproducibly observed chimeras with snoRNAs that have not previously been linked to U2 ($n=24$) and U6 ($n=17$) (Fig. S6J). Interestingly, we noted that many of candidate interactions lack chimeric support in FBL pulldown, contained snoRNAs that have been shown to target modifications on other snRNAs, and (for U2 chimeras) had a stereotypical positioning of NOLC1 chimeras in the central region of U2 which overlaps the Sm binding region (Fig. 5), S6K-L), suggesting that these unique chimeras in NOLC1 pulldown may reflect the more general role of NOLC1 in snRNA biogenesis [54, 55] rather than mediating methylation at this site. In summary, these results suggest that chimeric eCLIP can successfully enrich for previously characterized snoRNA interactions, as well as provide further depth to identify and understand novel interactions driven by non-canonical snoRNP complexes.

SNORD89 mediates U2 processing to fine-tune splice site recognition

To test whether integration of NOLC1 and FBL chimeric experiments could reveal biological insights into U2 function, we performed further studies of one poorly characterized snoRNA with strong chimeric signal in NOLC1 and FBL experiments, SNORD89. While NOLC1 captured SNORD89:U2 chimeras throughout U2 (with an enrichment in the central Sm binding region), FBL and NOP56 captured SNORD89:U2 chimeras primarily at the 5' end of U2 (Figs. 3C and 5J), overlapping the G11 and G12 Nm target sites that are responsive to SNORD89 knockdown (Fig. 3G). The functional impact of U2 modification at these specific nucleotides remains unclear: methylation at G12 was shown to be essential for splicing progression on a single pre-mRNA *in vitro* [48] but has not been explored on transcriptome-wide *in vivo*, and the role of G11 methylation is unknown. Thus, we next wanted to examine the functional impact of SNORD89 loss on spliceosomal activity.

To quantify the effect of SNORD89 on splicing in human cells, we performed SNORD89 ASO knockdown in 293T cells (Fig. 6A), followed by RNA-seq. Analysis of alternative splicing with rMATS identified 300 cassette exons in 298 genes more excluded upon SNORD89 knockdown (“knockdown-excluded exons”) and 334 cassette exons in 328 genes more included upon SNORD89 knockdown (“knockdown-included exons”) (Fig. 6B), confirming that SNORD89 significantly alters splicing. In further analysis where for each exon we calculated percent spliced in (PSI) as the ratio of the number of splice junction-overlapping reads that support exon inclusion divided by the number that support either exon inclusion or exclusion, we noted that SNORD89 preferentially regulates exons with nearly constitutive splicing — 60% of knockdown-excluded exons had PSI values of 0.95 or higher in control samples, and 66% of knockdown-included exons had PSI values of 0.95 or higher upon SNORD89 ASO (Fig. 6C). Although these were sometimes simple cassette exons (Fig. S7A-B), individual inspection indicated that

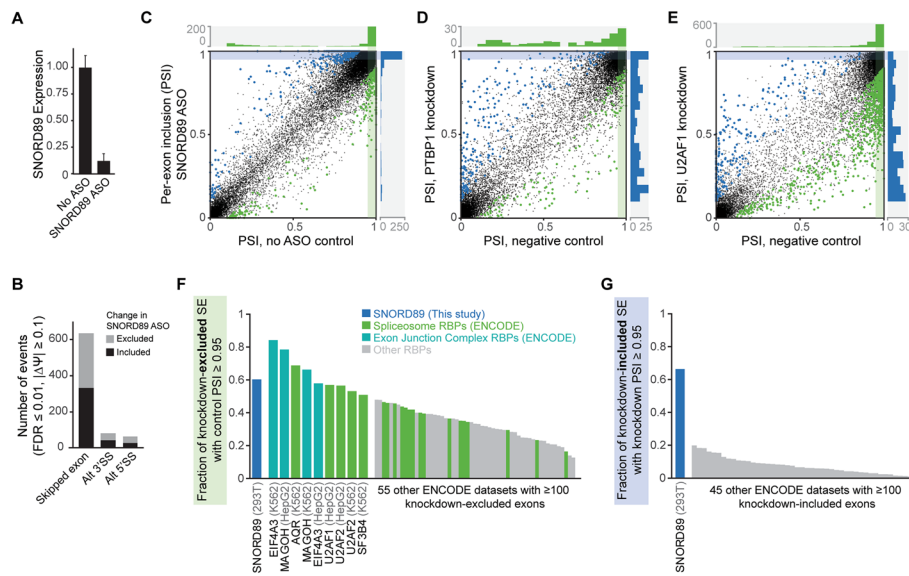


Fig. 6 SNORD89, a guide for U2 2'-O-methylation, plays a unique role in splicing control. **A** Bars indicate SNORD89 expression (from RT-qPCR) upon SNORD89 antisense oligonucleotide knockdown. **B** Bars indicate the number of significantly altered alternative splicing events from rMATS (FDR \leq 0.01, change in percent spliced in ($\Delta\Psi$) \geq 0.1, with \geq 10 junction reads in all samples), from RNA-seq comparing SNORD89 ASO versus no ASO control (2 replicates each). **C–E** Scatter plots indicate percent spliced in (Ψ) for (black) all exons, (green) knockdown-excluded, and (blue) knockdown-included cassette exons for **C** SNORD89, **D** PTBP1, and **E** U2AF1 knockdown. PTBP1 and U2AF1 data were obtained from the ENCODE project. Histograms indicate the frequency of Ψ values (in 0.05 bins) for (green) the control sample for knockdown-excluded exons, or (blue) the knockdown sample for knockdown-included samples. **F,G** Bars indicate the percent of events with $\Psi \geq 0.95$ for **F** the control sample for knockdown-excluded exons, or **G** the knockdown sample for knockdown-included exons. Shown are (leftmost bar, blue) SNORD89 knockdown and (all other bars) all ENCODE RBP knockdown datasets with at least 100 significantly altered exons

these often included complex splicing patterns, including skipping or inclusion of multiple adjacent exons (Fig. S7C-D).

To consider whether the effect of SNORD89 on knockdown-excluded exons with high PSI values was unique, we performed re-analysis of 473 RBP knockdown datasets generated by the ENCODE consortium [29]. We observed that canonical alternative splicing regulators showed a more varied distribution of PSI values for knockdown-excluded exons whereas spliceosomal components showed a pattern similar to SNORD89. For example, only 20% (28 out of 143) of PTBP1-dependent exons had $\Psi \geq 0.95$ in controls (Fig. 6D), but 57% (571 out of 1003) of U2AF1-dependent exons had $\Psi \geq 0.95$ in controls (Fig. 6E). Indeed, considering all 64 ENCODE datasets with at least 100 knockdown-excluded exons, the observation that more than half of knockdown-excluded exons had $\Psi \geq 0.95$ in controls was only seen for RBPs that were core components of the spliceosome or exon junction complex (Fig. 6F). Thus, SNORD89 enables inclusion of a set of near-constitutive exons similar to core splicing machinery RBPs.

In contrast, similar analysis of knockdown-included exons across ENCODE datasets indicated that the preferential inclusion of near-constitutive exons upon regulator knockdown was a unique property of SNORD89, as no RBP knockdown from ENCODE showed more than 20% of knockdown-included exons with $\Psi \geq 0.95$

(Fig. 6G). Thus, rather than simply being essential for enabling recognition of constitutive splice sites, SNORD89-mediated modifications on U2 appear to play a more precise role in limiting complete inclusion of near-constitutive sites. Analysis of intron retention suggested a similar role: SNORD89 knockdown caused a 24.7% decrease in the overall fraction of intronic reads observed (from 7.4% in control to 5.6% in knockdown) (Fig. S7E) which was observed in genes both containing or lacking SNORD89 knockdown-altered cassette exons (Fig. S7F). Although genes containing SNORD89 knockdown-included exons also showed decreased exonic coverage, this was not observed for other gene sets (Fig. S7G), suggesting that the global decrease in intronic reads is not simply due to transcriptional repression or post-transcriptional RNA decay of RNAs with differential splicing in the SNORD89 knockdown. Intron-specific analysis of SNORD89 knockdown similarly showed only 253 retained introns with increased retention but 869 retained introns with increased splicing (Fig. S7H).

The observation that SNORD89 knockdown more often led to more efficient splicing of retained introns, coupled with SNORD89 knockdown causing both increased and decreased mis-splicing of near-constitutive cassette exons, suggested that SNORD89 might be playing a unique role in maintaining both accurate and inaccurate splicing of specific introns. To test this hypothesis, we queried whether SNORD89 knockdown altered the accuracy of utilizing known splice junctions. We observed that SNORD89 knockdown caused a 12% decrease in the frequency of unannotated splice junctions (Fig. S7I), indicating that SNORD89 is acting to maintain rather than suppress utilization of unannotated junctions. In sum, these results suggest that modifications directed by SNORD89 are not only essential for proper splicing but may also be playing a critical role in maintaining splicing errors at a subset of splice sites.

Discussion

SnoRNAs play crucial roles in the modification and processing of rRNA and snRNA, impacting fundamental cellular processes such as translation and splicing. Despite clear biological relevance, research efforts have failed to identify targets for many orphan snoRNAs, and the roles of snoRNA-associated proteins are not well characterized. To address these gaps in understanding, we implemented an improved chimeric eCLIP approach that enables deep and accurate profiling of snoRNA interactions in an RBP-dependent manner. This new approach resulted in increased depth of snoRNA:target chimeras relative to previous efforts to directly map snoRNA interactions [14, 15, 18, 28]. The high accuracy achieved (AUC > 97% in both human and mouse cell lines) allows for benchmarking against known targets and the characterization of novel interactions. Notably, this accuracy was achieved empirically without needing to model interaction complementarity as in previous work [28], enabling recovery of candidate interactions that may have non-canonical interaction dynamics.

Using stringent peak calling criteria, we identified novel snoRNA interactions, including those of orphan snoRNAs. For example, we called a high-confidence interaction between Snord101 and 28S rRNA as well as Snord89 and U2 snRNA. While similar interactions were detected in previous chimeric ligation sequencing approaches, the predicted Nm sites were either inaccurate or lacked experimental validation [13, 18]. We

confirmed the bona fide effect of Snord101 and Snord89 on guiding Nm modification at 28S-G3283 and U2-G11/G12, respectively, in snoRNA loss-of-function experiments. Additionally, we identified putative interaction sites for Snord14, Snord23, Snord62, and Snord90, each supported by high methylation scores measured by RiboMeth-seq at the expected targeted nucleotide. Some of these interactions also have experimental support in other recent studies [13, 14]. We also refine previous predictions; previous work that identified SNORD23:U6 chimeras proposed a candidate methylation site (U6-Um64) that has not yet been observed, whereas our analysis indicates D'-box positioning at U6-Am70, a previously observed LARP7-dependent methylation event [25]. We observed similar results across all core C/D snoRBPs, confirming the robustness of this approach.

Novel interactions showed increased use of less conserved D' box-associated antisense elements. For example, the interaction identified between Snord89 and U2 snRNA is associated with the D' box, featuring a "UUGC" motif that diverges from the canonical "CUGA" motif. Our observation that loss of Snord89 affects Nm levels at two neighboring nucleotides, including G11 which was previously predicted as a Scarna2 target site [56] and G12 which was shown to be a Snord89 target site in yeast [35], suggests that perhaps the poorly conserved D' box motif may support more flexibility in the targeted nucleotide. This observation of a single snoRNA affecting methylation of neighboring nucleotides is a unique finding; whether additional snoRNAs have similar flexibility remains to be determined.

Modifications at the 5' end of U2 snRNA are crucial for snRNP assembly and splicing [48, 57]. However, their exact functions remain unclear, in part due to a lack of appropriate systems and tools. Our analysis indicated a unique role for U2-G11/G12-modifying SNORD89 in modulating spliceosome activity (Fig. 6). SNORD89 knockdown caused increased skipping of many normally constitutive exons, consistent with the previously described essential role for U2-G12 in splicing [48]. Surprisingly, we also observed 222 splicing events that were near-constitutive only upon SNORD89 knockdown, suggesting that these methylations also act to inhibit splicing of otherwise efficiently recognized exons. This pattern was not observed in any of 433 RBP knockdowns performed by the ENCORE project, suggesting these modifications may play a relatively unique role in splicing control. How altering U2-G11 and U2-G12 modification state could both mimic essential spliceosomal proteins as well as uniquely suppress inclusion of near-constitutive exons is unclear, but their position suggests a possible mechanism through a role in spliceosomal structure. Prior to the first transesterification step of splicing, U2 and U6 form intra- and inter-molecular structures through base-pairing interactions that facilitate active site formation and prime the spliceosome for nucleophilic attack [58–60]. The U2:U6 interactions can take on two different conformations, a three-way junction (3WJ) or a four-way junction (4WJ), and U2-G11 and U2-G12 are strategically positioned at the interface where the 3WJ or 4WJ structures forms [61–64]. Although the functional significance of these structures for splicing remains controversial, SNORD89 methylation of either or both U2-G11 and U2-G12 could be a novel mechanism through which small RNAs and RNA methylation can fine-tune splicing kinetics by mediating the intermediate spliceosome steps that occur stepwise prior to catalytic activation [63–65].

Further careful biochemical work will be required to explore the dynamics of structures, and how U2-G11 and U2-G12 modification alter these kinetics to drive splicing changes.

Beyond the core snoRBPs, numerous studies have indicated that additional accessory RBPs can interface with snoRNAs to modulate their targets or functions [24, 26]. Using snoRNA-associated accessory proteins as baits in chimeric eCLIP, we confirmed that WDR43, UTP18, LARP7, and NOLC1 associate with a specific subset of snoRNA interactions. We observed chimeric reads with SNORD3 at various processing sites within the 5' ETS regions of 45S pre-rRNA were particularly enriched with SSU processome RBPs rather than core snoRBPs, and these interactions illustrate how SNORD3 might arrange pre-rRNA folding via multiple interaction sites during early rRNA processing. We also observed U6 interactions with the specific snoRNAs through both LARP7 and FBL, validating the previous model that LARP7 bridges U6 modifications [25, 49]. Beyond that, we observed FBL-independent U2 interactions through accessory proteins, NOLC1. NOLC1 pulldown captured novel interactions at stereotypical positions (Sm binding site) in U2, suggesting these interactions may not drive canonical modifications. Although we do not yet know the function of these novel pairings, it is possible that they function as intermediates in enabling proper localization and targeting of these snoRNAs to their functional targets. Further experiments are required to understand the functions of such interactions on either U2 or other RNA molecules.

Although we successfully captured C/D snoRNA interactions by chimeric eCLIP, we were less successful at capturing H/ACA snoRNA interactions. Since we observed that eCLIP of DKC1 and other H/ACA snoRBPs successfully enriched for both H/ACA snoRNAs and (pre- and mature) rRNA, the inefficient capture of H/ACA snoRNA:target chimeras likely reflects a technical challenge of chimeric ligation. H/ACA snoRNAs contain longer stretches of both inter- and intra-molecular double-stranded RNA structure that may impair the flexibility necessary to support not only chimeric ligation, but also UV crosslinking and RNA fragmentation. We anticipate that the continued development of additional crosslinking reagents, RNA ligase enzymes, and reaction conditions will likely allow for successful capture of H/ACA interactions with a similar methodology.

Our chimeric eCLIP approach currently lacks identification of non-rRNA/snRNA targets, which could likely be improved by implementing rRNA depletion during library preparation — a strategy successfully employed in previous studies [10, 13]. Despite this limitation, our study successfully identified numerous novel interactions. These findings underscore the robustness of the chimeric eCLIP method and its ability to uncover significant snoRNA-target interactions, offering valuable insights into snoRNA functionality. Moving forward, future studies could also explore the use of different biological tissues or conditions to determine if snoRNA interactions vary across different biological contexts, providing a more comprehensive view of snoRNA functions.

Conclusions

Our study outlines a comprehensive framework for analyzing snoRNA-target interactions in an RNA-binding protein-dependent manner using chimeric eCLIP. Employing core C/D-box snoRNA-binding proteins, we accurately mapped known snoRNA interactions and identified target sites for orphan snoRNAs in both human and mouse cells. Utilizing less-studied snoRNA accessory RBPs, we enriched distinct snoRNA subsets,

revealing both canonical and non-canonical interactions. Finally, we describe how SNORD89 induces methylation of G11 and G12 sites on U2 spliceosomal RNA, which appears to be critical for fine-tuning exon inclusion. Collectively, our findings underscore the utility of chimeric eCLIP in mapping the snoRNA interactome, highlighting its potential for further exploration in snoRNA biology.

Methods

Cell culture

293T (632180, Takara), K562 (ATCC), and HepG2 (ATCC) cell lines were purchased from commercial suppliers and were not further authenticated. 293 T cells were cultured in DMEM (Thermo Fisher Scientific) supplemented with 10% FBS (Cytivia). Mouse ESC lines used in this study were derived from an *M. musculus* (129/Sv) × *M. castaneus* cross and have integrated EF1 α -rtTA and TetO-Ngn2 constructs. For routine passaging, mESCs were maintained on plates pre-coated with 0.2% gelatin in DMEM (Thermo) supplemented with 10 mM HEPES (Thermo), 0.11 mM β -mercaptoethanol (Sigma), 1X nonessential amino acids (Corning), 2 mM L-glutamine (Corning), 15% fetal bovine serum (Cytivia), and 1000 U/mL leukemia inhibitory factor (LIF; Sigma). All cell lines were maintained in a humidified 5% CO₂ incubator at 37°C, and cell lines were crosslinked as previously described [30]. Cells were not routinely screened for mycoplasma.

eCLIP library preparation

eCLIP was performed as previously described [66] using antibodies against FBL (A303-891A, Fortis Life Sciences), DKC1 (GTX109000, GeneTex), NOP56 (A302-721A, Fortis Life Sciences), NOP58 (A302-718A, Fortis Life Sciences), SNU13 (A304-030A, Fortis Life Sciences), NHP2 (15128-1-AP, Proteintech), NOP10 (ab134902, Abcam), and GAR1 (11711-1-AP, Proteintech) in K562, 293T, or HepG2 cells as indicated. For all above proteins, immunoprecipitation and western blot were performed with the same antibody. Samples were sequenced on the Illumina Novaseq X Plus platform.

eCLIP analysis

eCLIP data was analyzed using a previously described pipeline, including adapter trimming (cutadapt v3.4), removal of reads mapping to repetitive elements (STAR_2.4.0j), and mapping (STAR_2.4.0j) to the human genome (hg19) [66]. Quantitation of reads mapping to snoRNA and other repeat elements was performed according to a previously described analysis pipeline [37], using an updated database of snoRNA annotations generated by obtaining snoDB v1 [67] and removing duplicates. To compare against other RBPs, the updated snoRNA annotations were used to re-analyze all 223 eCLIP datasets (150 RBPs) generated by the ENCODE consortium [29]. snoRNA fold enrichment was calculated as reads per million in IP versus matched INPUT. For analyses comparing individual snoRNA fold-enrichment, snoRNAs with less than 5 reads in the IP sample were not included. RBP functional annotations were taken from the ENCODE analysis [37], and rRNA processing annotations were obtained from previous studies [68]. Fraction of RNA reads and enrichments

shown in Fig. 1 and Fig. S1 were obtained by averaging the reads per million across two replicates. Relative entropy (Kullback–Leibler divergence) of each element in each replicate was calculated as $p_i \times \log_2(\frac{p_i}{q_i})$, where p_i and q_i are the fraction of total reads in IP and input respectively that map to element i .

Chimeric eCLIP library preparation

The chimeric eCLIP method is based off of the previously described miRNA chimeric eCLIP protocol [32] with modifications as described below (see Additional file 4. snoRNA chimeric eCLIP Protocol for full step-by-step protocol). Briefly, 3 million cells were crosslinked with UV (254 nm, 400 mJ/cm²) to stabilize RNA-binding protein (RBP)-RNA interactions, followed by lysis, sonication and limited digestion with RNase I (Ambion). RBP-RNA complexes were immunoprecipitated overnight with a primary antibody of interest (5 µg) precoupled to magnetic secondary antibody beads (typically 200 µl M-280 Sheep Anti-Rabbit IgG Dynabeads, Thermo). Antibodies used were mostly identical to those used for eCLIP, including FBL (A303-891A, Fortis Life Sciences), DKC1 (GTX109000, GeneTex), NOP56 (A302-721A human and A302-720A mouse, Fortis Life Sciences), NOP58 (A302-718A, Fortis Life Sciences), GAR1 (11711-1-AP, Proteintech), ZC3H8 (A303-089A, Fortis Life Sciences), NOLC1 (A303-184A, Fortis Life Sciences), and LARP7 (A303-723A, Fortis Life Sciences); SMNDC1 used a different antibody (A302-836, Fortis Life Sciences) as the antibody used for eCLIP by the ENCODE consortium is no longer commercially available. Two percent of sample was saved as for paired input control, with the remainder used for immunoprecipitation. After washing with low- and high-salt buffer, the 3' end of RNA fragments was dephosphorylated with FastAP (Thermo) and T4 PNK (NEB), followed by 5' end phosphorylation of cleaved target RNAs with T4 polynucleotide kinase (PNK, 3'-phosphatase minus, NEB)). Chimeric ligation was then performed on beads at room temperature for 1 h with T4 RNA ligase (NEB) without adapters. After additional dephosphorylation steps (FastAP, T4 PNK), phosphorylated RNA adapter was ligated to the 3' end (T4 RNA Ligase, NEB). Samples were then denatured with 1X NuPage buffer (Life Technologies) and DTT, run on 4–12% Bis–Tris protein gels and transferred to nitrocellulose membranes (GE Amersham). The region from the observed protein size to 75 kD above (corresponding to ~250 nt RNA) was then isolated from membrane by razor blade, and RNA was isolated by Proteinase K (NEB) treatment followed by column purification (Zymo). RNA was then reverse transcribed with SuperScript IV Reverse Transcriptase (Invitrogen) using manganese chloride-based buffer to enhance read-through of modified nucleotides [69]. Excess primers were removed with ExoSAP-IT (Thermo), and RNA was degraded by alkaline hydrolysis, followed by RNA purification (MyOne Silane beads, Thermo). Next, a 5' Illumina DNA adapter was ligated to the 3' end of cDNA fragment with T4 RNA ligase HC enzyme on beads overnight. After beads cleanup, an aliquot of each sample was proceeded for qPCR to identify the proper PCR cycles. The remainder of the samples were amplified with bar-coded Illumina primers (Q5, NEB) and size selected via AMPure XP beads and 2% agarose gel (195–350 bp). Samples were then quantified by Agilent TapeStation and

sequenced either on the Illumina NextSeq (150 bp SE), NovaSeq X Plus (150 bp PE), or NovaSeq 6000 (75 bp SE) platforms.

Immunoprecipitation efficiency was tested by western blot using indicated protein antibodies at 0.2–0.5 µg/ml and Mouse or Rabbit TrueBlot secondary antibody at 1:4000.

Chimeric eCLIP mapping

The pipeline for analysis of chimeric eCLIP datasets is available at GitHub: <https://github.com/VanNostrandLab/snoRNA-chimeric> [70] and deposited on Zenodo: <https://doi.org/https://doi.org/10.5281/zenodo.14804082> [71], and the step-by-step pipeline is shown in Fig. S2A. Briefly, after demultiplexing using `umi_tools` (v1.1.1) to remove unique in-line barcode (10 random nucleotides), which was saved to read name for later use, adapter trimming was performed by `cutadapt` (v3.2). Next, the trimmed reads were mapped against human elements in RepBase with STAR (v2.4.0j), the reads unmapped to RepBase were then proceeded for the human genome (hg19) mapping with STAR (v2.4.0j). To remove the nonchimeric reads as much as possible, the stringent EndToEnd genomic alignment was performed and the chimeric reads with different region fragments ligated could not be aligned to genome. Those unmapped reads were then first mapped to snoRNA sequences compiled from human snoDB (v1) or mouse in-house annotations (Additional file 3: Table S2) using `bowtie2` (v2.2.5). The aligned snoRNA sequences were then filtered. The fragments aligned to snoRNAs over 18 nucleotides would be kept and if one read have multiple alignment results, only the reads with the maximum alignment score and longest length will be saved. In each of these reads, the remaining fragment that could not be aligned to snoRNA and over 18 nucleotides were saved as potential target regions. The potential target regions were then mapped against snoRNA sequences again to remove snoRNA: snoRNA interactions. The remaining reads were mapped to target RNA sequence (ribosomal RNA, small nuclear RNA, and tRNA) separately using `bowtie` (v1.3.0). Only the fragments mapped to target RNAs longer than 16 nucleotides and the gap between snoRNA aligned sequence and target RNA aligned sequence less than 4 were considered as real chimeric reads. Lastly, if the target fragments could not be aligned to any reference sequence, they would be merged and mapped to human (hg19) or mouse (mm10) using STAR. PCR duplicates were removed by comparing in-line barcode, sequence, snoRNA mapping location, and target RNA mapping location. Unless otherwise indicated, snoRNA enrichments from FBL chimeric eCLIP in HepG2 shown were obtained by averaging the reads per million across two replicates.

Chimeric eCLIP peak analysis

Peak calling was performed on individual snoRNA:target mapped files using Clipper [66]. To improve peak calling on edges of transcripts, all mapped chimeric rRNA/snRNA/tRNA read files, as well as the coordinates in the CLIPper reference files were “padded” (i.e., each start/end coordinate was extended by 30 nt) in silico. Peak calling on the genome was performed without padding. Immediately adjacent Clipper peaks were merged and considered as a single peak. Peak normalization was then performed

using “overlap_peakfi_with_bam.pl” script from the seCLIP pipeline [66]. Sequencing files from the input sample were processed according to the standard eCLIP pipeline and used as a background model for peak normalization. The input files were also padded prior to normalization, as processed with the IP files. Upon peak calling, the rRNA/snRNA/tRNA peak files were then “depadded” to the original positions. Peaks mapped to the genome were further subjected to filtering to discard any peaks corresponding to rRNA, snoRNA, or snRNA repeats that have escaped the genome masking process.

The “known” human snoRNA:target interactions were assigned based on snoDB. The mouse interactions were assigned based on previous literature [47, 72–76] and is summarized in Additional file 3: Table S2. High-confidence peaks were determined using parameters such as peak fold enrichment in the IP relative to the input (peak $fc > 3$) and fraction of reads at each peak for a given snoRNA (peak fraction > 0.1). To test whether the “peak fraction” criteria are suitable for classifying previously known positive interactions, an ROC was constructed using “pROC” R package [77] and rRNA peaks. The peak fraction threshold was selected to minimize the false positive rate.

Prediction of D/D' box position and base pairing region

For D box prediction, a regular expression was used to match the last occurrence of the exact CTGA consensus motif for each snoRNA in the annotation. For D' box prediction, multi-tier regular expression was used to match all occurrence of variations of D box motifs observed in annotated snoRNAs (i.e., CTGA, ATGA, GGTG, GTGG, GTGA, CTTA, CCGA, TCGA, CAGA, TGCA, AGGA, and TGTA) and putative antisense element was extracted 20 nt upstream of each potential D/D' box. In the rare cases where no motif was found, regions downstream of the C box motif (GATGA) were used to assess base complementarity with the chimeric target peak. The base pairing region was determined using the in silico tool, RNAplex, to assess the complementarity between all the putative antisense elements and the significant peaks (i.e., input normalized merged CLIPper peaks with peak fold change > 3 and peak fraction > 0.1). The antisense element that showed base pairing close to the D/D' box, with low energy and high complementarity proximal to the D/D' box was selected as the putative antisense element.

Antisense oligonucleotides

Gapmer ASOs of 20 nucleotides in length were synthesized and purified by IDT. A central gap segment comprising ten 2'-deoxynucleotides was flanked on the 5' and 3' wings by five 2'-MOE modified nucleotides. All internucleoside linkages were phosphorothioate.

Antisense oligonucleotide treatment of mESCs

For ASO experiments, mESC were first subject to in vitro neuron differentiated followed by free uptake of ASO, as follows. mESC were cultured for 24 h on gelatin-coated plates in neuron differentiation media [BrainPhys neuronal medium (Stem Cell Technologies) supplemented with 1X NeuroCult SM1 (Stem Cell Technologies), 1X N2 supplement (Thermo), 20 ng/mL brain-derived neurotrophic factor (Stem Cell Technologies)] containing 1 μ g/mL doxycycline (Sigma) to induce Ngn2 expression. Then, cells were

re-plated onto 0.1% PEI-coated dishes in neuron differentiation media containing 1 µg/mL doxycycline (Sigma). Within 24 h of re-plating, gapmer ASOs (IDT) were added to the culture media at a final concentration of 10 µM to allow for free uptake by the neurons. RNA was extracted 72 to 96 h after addition of the ASO using TRIzol (Thermo). The ASO sequences were Snord101 ASO 5'-GGGTATCCGACAATTCAAGT-3' and Snord89 ASO 5'-TGA CT CGCTTCAGGAGGTTT-3'.

Antisense oligonucleotide treatment of 293T cells

293T cells were transfected with 70 nM of gapmer ASO (IDT) using Lipofectamine RNAiMAX Transfection Reagent (Thermo). Cell culture media was replaced 24 h after transfection, and RNA was isolated 48 h after transfection using TRIzol (Thermo). The ASO sequence was SNORD89 ASO: 5'-TCGCTTCAGGATATTTTGTC-3'.

RT-qPCR

RT-qPCR reactions of 12.5 ng DNase-treated RNA were prepared using the iTaq™ Universal SYBR® Green One-Step Kit (Bio-Rad) and run on the Bio-Rad CFX Opus 384 Real-Time PCR System. Relative expression was calculated using the delta-delta Ct method relative to U6 snRNA (for mESC experiments) or 5S rRNA (for 293T experiments). The primers were Snord101 (ms) 5'-GTTTGCATGATGACTTGAATTG -3' / 5'-GTTTGT CAGACTAGCTGTTTC-3', Snord89 (ms) 5'-CGAATTGCAGTGTCTCCATC-3' / 5'-TGA CT CGCTTCAGGAGGTTT-3', U6 (ms) 5'-CTTCGGCAGCACATA TACTAAAA-3' / 5'-ATTTGCGTGTCATCCTTGCG-3', SNORD89 (hu) 5'-AAAAGG CCGAATTGCAGTGT-3' / 5'-GGTCAGACTAGTGGTTCGCT-3', and 5S rRNA (hu) 5'-GCCATACCACCCTGAACG-3' / 5'-AGCCTACAGCACCCGGTATT-3'.

RiboMeth-seq (RMS)

RMS library preparation and bioinformatic analyses were conducted as described previously [34, 78]. One hundred fifty to 250 ng of DNase-treated RNA was hydrolyzed in 50 mM sodium bicarbonate buffer (pH 9.2) for 1 to 12 min. The hydrolysis reaction was quenched in 1 mL EtOH containing 10 µL 3 M NaOAc, pH 5.2 (Thermo) and 15 µg Glycoblue coprecipitant (Thermo) and submerged in liquid nitrogen. Hydrolyzed RNA was then precipitated and washed in 80% EtOH. The intended fragment size of around 50–100 bp was verified on the TapeStation 4200 system (Agilent). RNA was dephosphorylated by Antarctic Phosphatase (New England Biolabs) for 30 min at 37 °C, and end-repaired by T4 PNK (New England Biolabs) in the presence of 1 mM ATP (New England Biolabs) for 1 h at 37 °C. End-repaired RNA was purified using RNA Clean & Concentrator-5 columns (Zymo). Illumina libraries were then prepared using the NEB-Next® Multiplex Small RNA Library Prep Set for Illumina® kit (New England Biolabs) and purified on NucleoSpin® Gel and PCR Clean-up columns (Takara Bio). Illumina sequencing of the libraries was performed on HiSeq (50 bp SE) or NovaSeq (SE100 or PE100) platforms.

RNA-seq analysis of SNORD89 knockdown

PolyA-selected RNA-seq libraries were prepared by Novogene and sequenced on the Illumina NovaSeq (150 bp PE) platform. After adapter trimming (cutadapt v3.4), reads were first mapped (STAR, v2.4.0j) against a database of repetitive elements (RepBase v18.05), with aligned reads removed. Unmapped reads were then mapped (STAR v2.4.0j) against the human genome (hg19). Alternative splicing was quantitated with rMATS-Turbo (v4.3.0) [79] for SNORD89 ASO versus no-ASO control. Unannotated junctions were defined as splice junctions identified in STAR mapping that were not present in Gencode v19 annotations (specifically, gencode.v19.chr_patch_hapl_scaff) or Incipedia (v5.0) [80]. ENCODE RBP knockdown data was obtained from the ENCODE Consortium [29].

Intron retention analysis

Reads were trimmed using cutadapt v1.14 [81] with parameters `-m 20 -u 3 -q 20,0 --nextseq-trim=5 --max-n 0`. Reads were aligned to the human reference genome (build GRCh38) using STAR [82] v2.5.4a with parameters `--outFilterMultimapNmax 101 --outSJfilterOverhangMin 3 1 1 1 --outSJfilterDistToOtherSJmin 0 0 0 0 --alignIntronMin 11`. Uniquely mapped reads were extracted using samtools [83] `view -q 255`. For measuring per-intron retention, we determined the splicing status of each read spanning splice junctions using the CIGAR string and custom scripts from <https://github.com/churchmanlab/nano-COP> [84]. The splicing index was then computed as $(\text{number of spliced reads} * 2) / \text{number of unspliced reads}$. Introns covered by > 20 splice junction reads were included in the analysis. Splicing indices between no ASO control and SNORD89 knockdown were compared using rMATS-stat (<https://github.com/Xinglab/rMATS-STAT>) with a significance threshold of $\text{FDR} < 0.05$ and a splicing index $\log_2(\text{fold change}) (\text{SNORD89 KD} / \text{control}) > 1$ or < -1 .

Supplementary Information

The online version contains supplementary material available at <https://doi.org/10.1186/s13059-025-03508-7>.

Additional file 1: Supplementary figures: Fig S1-S7.
Additional file 2: Significant peaks from snoRNA chimeric analysis.
Additional file 3: Mouse snoRNA annotation database.
Additional file 4: snoRNA chimeric eCLIP step-by-step protocol.

Acknowledgements

We thank the Bauer Core Facility at Harvard University for technical support and access to high-throughput sequencing instrumentation. We want to thank all members of the Whipple and Van Nostrand labs for valuable discussions. This project was supported in part by the Genomic and RNA Profiling Core at Baylor College of Medicine with funding from the NIH NCI (P30CA125123) and CPRIT (RP200504) grants and in part by the Cancer Genomics Center at University of Texas Health with funding by the Cancer Prevention and Research Institute of Texas (CPRIT RP180734).

Peer review information

Claudia Feng was the primary editor of this article and managed its editorial process and peer review in collaboration with the rest of the editorial team. The peer review history is available in the online version of this article.

Authors' contributions

Z.S., B.B., A.J.W., and E.L.V.N. conceptualized the project and methodology, Z.S., B.B., S.S., F.Y., T.D.Z., M.V.A., C.L.R., and K.C. performed investigation and formal analysis, Z.S., B.B., A.J.W., and E.L.V.N. wrote the main manuscript text, A.J.W. and E.L.V.N. performed review and editing of the text, and A.J.W. and E.L.V.N. supervised and acquired funding for the work. All authors read and approved the final manuscript.

Funding

This work was supported by funding from the National Institute of General Medical Sciences (F32GM156080 (B.B.) and R35GM146921 (A.J.W.)) and the National Human Genome Research Institute (R00HG009530 (E.L.V.N.) and R35HG011909 (E.L.V.N.)). Additional support came from the Klingenstein-Simons Fellowship Award in Neuroscience (A.J.W.), the George W. Merck Fellowship Fund (A.J.W.), and the Rita Allen Foundation (A.J.W.).

Data availability

The datasets supporting the conclusions of this article have been deposited in the Gene Expression Omnibus under accession identifiers GSE277413 (RNA-seq) [85], GSE277414 (chimeric eCLIP) [86], GSE277416 (eCLIP) [87], and GSE277419 (Ribo-Meth-seq) [88]. The pipeline for analysis of chimeric eCLIP datasets is available at GitHub: <https://github.com/VanNostrandLab/snoRNA-chimeric> [70] and deposited on Zenodo: <https://doi.org/10.5281/zenodo.14804082> [71].

Declarations**Ethics approval and consent to participate**

Not applicable.

Consent for publication

Not applicable.

Competing interests

ELVN is co-founder, member of the Board of Directors, on the SAB, equity holder, and paid consultant for Eclipse BioInnovations, on the SAB of RNAConnect, and is inventor of intellectual property owned by University of California San Diego. ELVN's interests have been reviewed and approved by the Baylor College of Medicine in accordance with its conflict of interest policies. The other authors declare no competing interests.

Received: 20 September 2024 Accepted: 13 February 2025

Published online: 25 February 2025

References

- Massenet S, Bertrand E, Verheggen C. Assembly and trafficking of box C/D and H/ACA snoRNPs. *RNA Biol.* 2017;14:680–92.
- Taoka M, Nobe Y, Yamaki Y, Sato K, Ishikawa H, Izumikawa K, et al. Landscape of the complete RNA chemical modifications in the human 80S ribosome. *Nucleic Acids Res.* 2018;46:9289–98.
- Yelland JN, Bravo JPK, Black JJ, Taylor DW, Johnson AW. A single 2'-O-methylation of ribosomal RNA gates assembly of a functional ribosome. *Nat Struct Mol Biol.* 2023;30:91–8.
- Polikanov YS, Melnikov SV, Söll D, Steitz TA. Structural insights into the role of rRNA modifications in protein synthesis and ribosome assembly. *Nat Struct Mol Biol.* 2015;22:342–4.
- Khoshnevis S, Dreggors-Walker RE, Marchand V, Motorin Y, Ghalei H. Ribosomal RNA 2'-O-methylations regulate translation by impacting ribosome dynamics. *Proc Natl Acad Sci.* 2022;119:e2117334119.
- Lowe TM, Eddy SR. A computational screen for methylation guide snoRNAs in yeast. *Science.* 1999;283:1168–71.
- Kehr S, Bartschat S, Stadler PF, Tafer H. PLEXY: efficient target prediction for box C/D snoRNAs. *Bioinformatics.* 2011;27:279–80.
- Deschamps-Francoeur G, Couture S, Abou-Elela S, Scott MS. The snoGloBe interaction predictor reveals a broad spectrum of C/D snoRNA RNA targets. *Nucleic Acids Res.* 2022;50:6067–83.
- Tafer H, Kehr S, Hertel J, Hofacker IL, Stadler PF. RNAsnoop: efficient target prediction for H/ACA snoRNAs. *Bioinformatics.* 2010;26:610–6.
- Nguyen TC, Cao X, Yu P, Xiao S, Lu J, Biase FH, et al. Mapping RNA-RNA interactome and RNA structure in vivo by MARIO. *Nat Commun.* 2016;7:12023.
- Aw JGA, Shen Y, Wilm A, Sun M, Lim XN, Boon K-L, et al. In vivo mapping of eukaryotic RNA interactomes reveals principles of higher-order organization and regulation. *Mol Cell.* 2016;62:603–17.
- Lu Z, Zhang QC, Lee B, Flynn RA, Smith MA, Robinson JT, et al. RNA duplex map in living cells reveals higher-order transcriptome structure. *Cell.* 2016;165:1267–79.
- Sharma E, Sterne-Weiler T, O'Hanlon D, Blencowe BJ. Global mapping of human RNA-RNA interactions. *Mol Cell.* 2016;62:618–26.
- Dunn-Davies H, Dudnakova T, Langhendries J-L, Watkins N, Lafontaine DLJ, Tollervey D. Systematic mapping of small nucleolar RNA targets in human cells. *bioRxiv*; 2021. p. 2021.07.22.451324. Available from: <https://www.biorxiv.org/content/10.1101/2021.07.22.451324v1>. Cited 2023 Nov 17.
- Kudla G, Granneman S, Hahn D, Beggs JD, Tollervey D. Cross-linking, ligation, and sequencing of hybrids reveals RNA-RNA interactions in yeast. *Proc Natl Acad Sci.* 2011;108:10010–5.
- Tycowski KT, You Z-H, Graham PJ, Steitz JA. Modification of U6 Spliceosomal RNA Is Guided by Other Small RNAs. *Mol Cell.* 1998;2:629–38.
- Vitali P, Kiss T. Cooperative 2'-O-methylation of the wobble cytidine of human elongator tRNAMet(CAT) by a nucleolar and a Cajal body-specific box C/D RNP. *Genes Dev.* 2019;33:741–6.
- Zhang M, Li K, Bai J, Van Damme R, Zhang W, Alba M, et al. A snoRNA-tRNA modification network governs codon-biased cellular states. *Proc Natl Acad Sci.* 2023;120:e2312126120.
- Elliott BA, Ho H-T, Ranganathan SV, Vangaveti S, Ilkayeva O, Abou Assi H, et al. Modification of messenger RNA by 2'-O-methylation regulates gene expression in vivo. *Nat Commun.* 2019;10:3401.

20. Kishore S, Stamm S. The snoRNA HBII-52 regulates alternative splicing of the serotonin receptor 2C. *Science*. 2006;311:230–2.
21. Tycowski KT, Shu MD, Steitz JA. Requirement for intron-encoded U22 small nucleolar RNA in 18S ribosomal RNA maturation. *Science*. 1994;266:1558–61.
22. Liao H, Gaur A, McConie H, Shekar A, Wang K, Chang JT, et al. Human NOP2/NSUN1 regulates ribosome biogenesis through non-catalytic complex formation with box C/D snoRNPs. *Nucleic Acids Res*. 2022;50:10695–716.
23. Falaleeva M, Pages A, Matuszek Z, Hidmi S, Agranat-Tamir L, Korotkov K, et al. Dual function of C/D box small nucleolar RNAs in rRNA modification and alternative pre-mRNA splicing. *Proc Natl Acad Sci U S A*. 2016;113:E1625–34.
24. Huang C, Shi J, Guo Y, Huang W, Huang S, Ming S, et al. A snoRNA modulates mRNA 3' end processing and regulates the expression of a subset of mRNAs. *Nucleic Acids Res*. 2017;45:8647–60.
25. Hasler D, Meduri R, Bąk M, Lehmann G, Heizinger L, Wang X, et al. The alazami syndrome-associated protein LARP7 Guides U6 small nuclear RNA modification and contributes to splicing robustness. *Mol Cell*. 2020;77:1014–1031.e13.
26. Izumikawa K, Nobe Y, Ishikawa H, Yamauchi Y, Taoka M, Sato K, et al. TDP-43 regulates site-specific 2'-O-methylation of U1 and U2 snRNAs via controlling the Cajal body localization of a subset of C/D scaRNAs. *Nucleic Acids Res*. 2019;47:2487–505.
27. Kishore S, Gruber AR, Jedlinski DJ, Syed AP, Jorjani H, Zavolan M. Insights into snoRNA biogenesis and processing from PAR-CLIP of snoRNA core proteins and small RNA sequencing. *Genome Biol*. 2013;14:R45.
28. Gumienny R, Jedlinski DJ, Schmidt A, Gypas F, Martin G, Vina-Vilaseca A, et al. High-throughput identification of C/D box snoRNA targets with CLIP and RiboMeth-seq. *Nucleic Acids Res*. 2017;45:2341–53.
29. Van Nostrand EL, Freese P, Pratt GA, Wang X, Wei X, Xiao R, et al. A large-scale binding and functional map of human RNA-binding proteins. *Nature*. 2020;583:711–9.
30. Van Nostrand EL, Pratt GA, Shishkin AA, Gelboin-Burkhart C, Fang MY, Sundararaman B, et al. Robust transcriptome-wide discovery of RNA-binding protein binding sites with enhanced CLIP (eCLIP). *Nat Methods*. 2016;13:508–14.
31. Watkins NJ, Ségault V, Charpentier B, Nottrott S, Fabrizio P, Bachi A, et al. A common core RNP structure shared between the small nucleolar box C/D RNPs and the spliceosomal U4 snRNP. *Cell*. 2000;103:457–66.
32. Manakov SA, Shishkin AA, Yee BA, Shen KA, Cox DC, Park SS, et al. Scalable and deep profiling of mRNA targets for individual microRNAs with chimeric eCLIP. *bioRxiv*; 2022. p. 2022.02.13.480296. Available from: <https://www.biorxiv.org/content/10.1101/2022.02.13.480296v2>. Cited 2024 Jul 10.
33. Lovci MT, Ghanem D, Marr H, Arnold J, Gee S, Parra M, et al. Rbfox proteins regulate alternative mRNA splicing through evolutionarily conserved RNA bridges. *Nat Struct Mol Biol*. 2013;20:1434–42.
34. Marchand V, Blanloeil-Oillo F, Helm M, Motorin Y. Illumina-based RiboMethSeq approach for mapping of 2'-O-Me residues in RNA. *Nucleic Acids Res*. 2016;44:e135.
35. Deryusheva S, Talhouarne GJS, Gall JG. "Lost and Found": snoRNA Annotation in the *Xenopus* Genome and Implications for Evolutionary Studies. *Mol Biol Evol*. 2020;37:149–66.
36. Gawade K, Plewka P, Häfner SJ, Lund AH, Marchand V, Motorin Y, et al. FUS regulates a subset of snoRNA expression and modulates the level of rRNA modifications. *Sci Rep*. 2023;13:2974.
37. Van Nostrand EL, Pratt GA, Yee BA, Wheeler EC, Blue SM, Mueller J, et al. Principles of RNA processing from analysis of enhanced CLIP maps for 150 RNA binding proteins. *Genome Biol*. 2020;21:90.
38. Sondalle SB, Baserga SJ, Yelick PC. The contributions of the ribosome biogenesis protein Utp5/WDR43 to craniofacial development. *J Dent Res*. 2016;95:1214–20.
39. Dörner K, Ruggeri C, Zemp I, Kutay U. Ribosome biogenesis factors—from names to functions. *EMBO J*. 2023;42:e112699.
40. Zhang L, Lin J, Ye K. Structural and functional analysis of the U3 snoRNA binding protein Rrp9. *RNA*. 2013;19:701–11.
41. Kass S, Tyc K, Steitz JA, Sollner-Webb B. The U3 small nucleolar ribonucleoprotein functions in the first step of pre-ribosomal RNA processing. *Cell*. 1990;60:897–908.
42. Hunziker M, Barandun J, Petfalski E, Tan D, Delan-Forino C, Molloy KR, et al. UtpA and UtpB chaperone nascent pre-ribosomal RNA and U3 snoRNA to initiate eukaryotic ribosome assembly. *Nat Commun*. 2016;7:12090.
43. Zhang L, Wu C, Cai G, Chen S, Ye K. Stepwise and dynamic assembly of the earliest precursors of small ribosomal subunits in yeast. *Genes Dev*. 2016;30:718–32.
44. Dutca LM, Gallagher JEG, Baserga SJ. The initial U3 snoRNA:pre-rRNA base pairing interaction required for pre-18S rRNA folding revealed by in vivo chemical probing. *Nucleic Acids Res*. 2011;39:5164–80.
45. Swiatkowska A, Wlotzka W, Tuck A, Barrass JD, Beggs JD, Tollervey D. Kinetic analysis of pre-ribosome structure in vivo. *RNA*. 2012;18:2187–200.
46. Rodgers ML, Woodson SA. A roadmap for ribosomal RNA folding and assembly during transcription. *Trends Biochem Sci*. 2021;46:889–901.
47. Bohnsack MT, Sloan KE. Modifications in small nuclear RNAs and their roles in spliceosome assembly and function. *Biol Chem*. 2018;399:1265–76.
48. Dönmez G, Hartmuth K, Lührmann R. Modified nucleotides at the 5' end of human U2 snRNA are required for spliceosomal E-complex formation. *RNA*. 2004;10:1925–33.
49. Wang X, Li ZT, Yan Y, Lin P, Tang W, Hasler D, et al. LARP7-Mediated U6 snRNA Modification Ensures Splicing Fidelity and Spermatogenesis in Mice. *Mol Cell*. 2020;77:999–1013.e6.
50. Bizarro J, Deryusheva S, Wacheul L, Gupta V, Ernst FGM, Lafontaine DLJ, et al. Nopp140-chaperoned 2'-O-methylation of small nuclear RNAs in Cajal bodies ensures splicing fidelity. *Genes Dev*. 2021; Available from: <http://genesdev.cshlp.org/content/early/2021/07/21/gad.348660.121>. Cited 2023 Dec 1.
51. Eglhoff S, Vitali P, Tellier M, Raffel R, Murphy S, Kiss T. The 7SK snRNP associates with the little elongation complex to promote snRNA gene expression. *EMBO J*. 2017;36:934–48.
52. Rappsilber J, Ajuh P, Lamond AI, Mann M. SPF30 is an essential human splicing factor required for assembly of the U4/U5/U6 Tri-small nuclear ribonucleoprotein into the Spliceosome *. *J Biol Chem*. 2001;276:31142–50.

53. Zhu W, Zhou B, Rong L, Ye L, Xu H, Zhou Y, et al. Roles of PTBP1 in alternative splicing, glycolysis, and oncogenesis. *J Zhejiang Univ Sci B*. 2020;21:122–36.
54. Yang Y, Isaac C, Wang C, Dragon F, Pogačić V, Meier UT. Conserved Composition of Mammalian Box H/ACA and Box C/D Small Nucleolar Ribonucleoprotein Particles and Their Interaction with the Common Factor Nopp140. *Mol Biol Cell*. 2000;11:567–77.
55. Bizarro J, Bhardwaj A, Smith S, Meier UT. Nopp140-mediated concentration of telomerase in Cajal bodies regulates telomere length. *Mol Biol Cell*. 2019;30:3136–50.
56. Hüttenhofer A, Kieffmann M, Meier-Ewert S, O'Brien J, Lehrach H, Bachellerie JP, et al. RNomics: an experimental approach that identifies 201 candidates for novel, small, non-messenger RNAs in mouse. *EMBO J*. 2001;20:2943–53.
57. Yu YT, Shu MD, Steitz JA. Modifications of U2 snRNA are required for snRNP assembly and pre-mRNA splicing. *EMBO J*. 1998;17:5783–95.
58. Madhani HD, Guthrie C. A novel base-pairing interaction between U2 and U6 snRNAs suggests a mechanism for the catalytic activation of the spliceosome. *Cell*. 1992;71:803–17.
59. Wassarman DA, Steitz JA. A base-pairing interaction between U2 and U6 small nuclear RNAs occurs in > 150S complexes in HeLa cell extracts: implications for the spliceosome assembly pathway. *Proc Natl Acad Sci U S A*. 1993;90:7139–43.
60. Wu J, Manley JL. Base pairing between U2 and U6 snRNAs is necessary for splicing of a mammalian pre-mRNA. *Nature*. 1991;352:818–21.
61. Guo Z, Karunatilaka KS, Rueda D. Single-molecule analysis of protein-free U2–U6 snRNAs. *Nat Struct Mol Biol*. 2009;16:1154–9.
62. Sashital DG, Cornilescu G, Butcher SE. U2–U6 RNA folding reveals a group II intron-like domain and a four-helix junction. *Nat Struct Mol Biol*. 2004;11:1237–42.
63. Sidarovich A, Will CL, Anokhina MM, Ceballos J, Sievers S, Agafonov DE, et al. Identification of a small molecule inhibitor that stalls splicing at an early step of spliceosome activation. 2017;
64. Zhao C, Bachu R, Popović M, Devany M, Brenowitz M, Schlatterer JC, et al. Conformational heterogeneity of the protein-free human spliceosomal U2–U6 snRNA complex. *RNA*. 2013;19:561–73.
65. Townsend C, Leelaram MN, Agafonov DE, Dybkov O, Will CL, Bertram K, et al. Mechanism of protein-guided folding of the active site U2/U6 RNA during spliceosome activation. *Science*. 2020;370:eabc3753.
66. Blue SM, Yee BA, Pratt GA, Mueller JR, Park SS, Shishkin AA, et al. Transcriptome-wide identification of RNA-binding protein binding sites using seCLIP-seq. *Nat Protoc*. 2022;17:1223–65.
67. Bouchard-Bourelle P, Desjardins-Henri C, Mathurin-St-Pierre D, Deschamps-Francoeur G, Fafard-Couture É, Garant J-M, et al. snoDB: an interactive database of human snoRNA sequences, abundance and interactions. *Nucleic Acids Res*. 2020;48:D220–5.
68. Tafforeau L, Zorbas C, Langhendries J-L, Mullineux S-T, Stamatopoulou V, Mullier R, et al. The complexity of human ribosome biogenesis revealed by systematic nucleolar screening of Pre-rRNA processing factors. *Mol Cell*. 2013;51:539–51.
69. Van Nostrand EL, Shishkin AA, Pratt GA, Nguyen TB, Yeo GW. Variation in single-nucleotide sensitivity of eCLIP derived from reverse transcription conditions. *Methods*. 2017;126:29–37.
70. Song Z, Bae B, Schnabl S, Yuan F, De Zoysa T, Akinyi MV, et al. Processing pipeline for snoRNA-focused chimeric eCLIP. GitHub. 2025; Available from: <https://github.com/VanNostrandLab/snoRNA-chimeric>.
71. Song Z, Bae B, Schnabl S, Yuan F, De Zoysa T, Akinyi M, et al. Processing pipeline for snoRNA-focused chimeric eCLIP. Zenodo. 2025; Available from: <https://doi.org/10.5281/zenodo.14804082>
72. Hebras J, Marty V, Personnaz J, Mercier P, Krogh N, Nielsen H, et al. Reassessment of the involvement of Snord115 in the serotonin 2c receptor pathway in a genetically relevant mouse model. *eLife*. 2020;9:e60862.
73. Incarnato D, Anselmi F, Morandi E, Neri F, Maldotti M, Rapelli S, et al. High-throughput single-base resolution mapping of RNA 2'-O-methylated residues. *Nucleic Acids Res*. 2017;45:1433–41.
74. Yoshihama M, Nakao A, Kenmochi N. snOPY: a small nucleolar RNA orthological gene database. *BMC Res Notes*. 2013;6:426.
75. Sharma S, Marchand V, Motorin Y, Lafontaine DLJ. Identification of sites of 2'-O-methylation vulnerability in human ribosomal RNAs by systematic mapping. *Sci Rep*. 2017;7:11490.
76. Krogh N, Jansson MD, Häfner SJ, Tehler D, Birkedal U, Christensen-Dalsgaard M, et al. Profiling of 2'-O-Me in human rRNA reveals a subset of fractionally modified positions and provides evidence for ribosome heterogeneity. *Nucleic Acids Res*. 2016;44:7884–95.
77. Robin X, Turck N, Hainard A, Tiberti N, Lisacek F, Sanchez J-C, et al. pROC: an open-source package for R and S+ to analyze and compare ROC curves. *BMC Bioinformatics*. 2011;12:77.
78. Birkedal U, Christensen-Dalsgaard M, Krogh N, Sabarinathan R, Gorodkin J, Nielsen H. Profiling of ribose methylations in RNA by high-throughput sequencing. *Angew Chem Int Ed Engl*. 2015;54:451–5.
79. rMATS-turbo: an efficient and flexible computational tool for alternative splicing analysis of large-scale RNA-seq data | Nature Protocols. Available from: <https://www.nature.com/articles/s41596-023-00944-2>. Cited 2024 Sep 19.
80. Volders P-J, Anckaert J, Verheggen K, Nuytens J, Martens L, Mestdagh P, et al. LNCipedia 5: towards a reference set of human long non-coding RNAs. *Nucleic Acids Res*. 2019;47:D135–9.
81. Martin M. Cutadapt removes adapter sequences from high-throughput sequencing reads. *EMBnet J*. 2011;17:10–2.
82. Dobin A, Davis CA, Schlesinger F, Drenkow J, Zaleski C, Jha S, et al. STAR: ultrafast universal RNA-seq aligner. *Bioinformatics*. 2013;29:15–21.
83. Li H, Handsaker B, Wysoker A, Fennell T, Ruan J, Homer N, et al. The Sequence Alignment/Map format and SAMtools. *Bioinformatics*. 2009;25:2078–9.
84. Drexler HL, Choquet K, Merens HE, Tang PS, Simpson JT, Churchman LS. Revealing nascent RNA processing dynamics with nano-COP. *Nat Protoc*. 2021;16:1343–75.
85. Song Z, Bae B, Schnabl S, Yuan F, De Zoysa T, Akinyi MV, et al. GEO Accession_RNA seq. 2025. Available from: <https://www.ncbi.nlm.nih.gov/geo/query/acc.cgi?acc=GSE277413>.

86. Song Z, Bae B, Schnabl S, Yuan F, De Zoysa T, Akinyi MV, et al. GEO Accession_chimeric eCLIP. 2025. Available from: <https://www.ncbi.nlm.nih.gov/geo/query/acc.cgi?acc=GSE277414>.
87. Song Z, Bae B, Schnabl S, Yuan F, De Zoysa T, Akinyi MV, et al. GEO Accession_eCLIP. 2025. Available from: <https://www.ncbi.nlm.nih.gov/geo/query/acc.cgi?acc=GSE277416>.
88. Song Z, Bae B, Schnabl S, Yuan F, De Zoysa T, Akinyi MV, et al. GEO Accession_Ribo-Meth-seq. Available from: <https://www.ncbi.nlm.nih.gov/geo/query/acc.cgi?acc=GSE277419>.

Publisher's Note

Springer Nature remains neutral with regard to jurisdictional claims in published maps and institutional affiliations.